

RELIABLE EIGENSPACE ERROR ESTIMATION USING SOURCE ERROR ESTIMATORS

JAY GOPALAKRISHNAN AND GABRIEL PINOCHET-SOTO

Dedicated to the memory of Professor Raytcho Lazarov

ABSTRACT. We introduce a framework for repurposing error estimators for source problems to compute an estimator for the gap between eigenspaces and their discretizations. Of interest are eigenspaces of finite clusters of eigenvalues of unbounded nonselfadjoint linear operators with compact resolvent. Eigenspaces and eigenvalues of rational functions of such operators are studied as a first step. Under an assumption of convergence of resolvent approximations in the operator norm and an assumption on global reliability of source problem error estimators, we show that the gap in eigenspace approximations can be bounded by a globally reliable and computable error estimator. Also included are applications of the theoretical framework to first-order system least squares (FOSLS) discretizations and discontinuous Petrov-Galerkin (DPG) discretizations, both yielding new estimators for the error gap. Numerical experiments with a selfadjoint model problem and with a leaky nonselfadjoint waveguide eigenproblem show that adaptive algorithms using the new estimators give refinement patterns that target the cluster as a whole instead of individual eigenfunctions.

1. INTRODUCTION

When clusters of some physically relevant eigenvalues are to be approximated, eigensolvers often use functions on the complex plane to transform such eigenvalues to a dominant set of eigenvalues of the rational function of the operator. Shifted inverse iteration is perhaps the simplest example. Contour integral iterative solvers provide more involved examples. Such eigensolvers typically require many applications of the resolvent operator, which amounts to solving “source problems.” When using finite element methods for such source problems, one often has ready access to *a posteriori* error estimators for source problems. The goal of this work is to repurpose such source problem error estimators to give error indicators for the gap between discrete and exact eigenspaces of the targeted eigenvalue cluster.

Error estimation for eigenvalue problems is well-studied. In the extensive literature on this topic, one finds estimators for least-squares discretizations [7, 6], guaranteed bounds for eigenvalue clusters of selfadjoint problems [14, 15], homotopy methods for nonselfadjoint problems [20], Crouzeix-Raviart discretizations for the Laplace operator [17, 19], mixed methods [9], skeletal finite element methods [21], oscillation-free discretizations for symmetric operators [18], dual weighted residual methods [48, 62], explicit error estimators [55], and works targeting cluster error estimation [15, 35, 34]. Source problem error estimators have of course been studied even longer, see e.g., [1, 2, 3, 29, 46, 58, 67, 68]. The goal of this paper is to make it easy to reutilize source problem error estimators within an eigensolver. While our basic idea for eigenspace error estimation is not radically different from the cited previous literature, our focus on unbounded nonselfadjoint operators within the theory presented here

is new, and so is the practical perspective of repurposing source problem error estimators within often-used spectral mappings by rational functions.

In various practical scenarios, such as in our prior work on eigenmodes of microstructured optical fibers [37], the need arises to numerically approximate the eigenspace corresponding to a finite cluster Λ of physically interesting eigenvalues in the spectrum of an unbounded differential operator \mathcal{A} . These eigenvalues need neither be dominant nor lie near any extremity of the spectrum. Consider eigensolvers that target such clusters using a rational function $r(z)$ of a complex variable z , applied to the operator \mathcal{A} . The $r(\cdot)$ is usually designed to make $r(\Lambda)$ into a dominant set of eigenvalues of $r(\mathcal{A})$ so that standard iterative techniques can capture them easily. For example, the subspace iteration $E_{(\ell)} = r(\mathcal{A})E_{(\ell-1)}$ for $\ell = 1, 2, \dots$, starting with some initial space $E_{(0)}$, can be proven to converge to the wanted eigenspace under suitable conditions [38]. Of course, in practice, we must apply such eigensolvers to finite-dimensional approximations of $r(\mathcal{A})$, such as finite element approximations, which then capture a discretized eigenspace. We are interested in computable error estimators for such discrete eigenspaces that can be used as a basis for automatic adaptive algorithms. A key difference when compared to the standard adaptivity for source problems is that here the desired output is a *space*, a multidimensional eigenspace, rather than a single solution function. Accordingly, the reliability of our error estimator is established using the gap metric which gives a notion of distance between spaces. The main result, Theorem 3.10, bounds the gap between exact and approximate eigenspace by a computable error estimator.

A prominent example of the above-mentioned type of rational functions (that make the targeted portion of the spectrum into a dominant one) is the so-called “FEAST method” [38, 52, 60, 61]. It is a filtered subspace iteration, i.e., a subspace iteration using $r(\mathcal{A})$ where $r(\cdot)$ is viewed as a filter that isolates wanted portions of the spectrum. In such examples, it is essential to understand how the eigenspaces of $r(\mathcal{A})$ relate to those of \mathcal{A} since the subspace iteration captures the former. This requires us to tailor the spectral mapping theorem [49] to the case of a rational function of a linear operator. We provide elementary arguments clarifying how eigenspaces are transformed under $r(\cdot)$ by building on a result of Yamamoto [66] (which he proves very simply using Bézout’s identity). This first step (completed in the next section) then clarifies what assumptions we must place on the rational filters in the remainder of the analysis for nonselfadjoint \mathcal{A} . We then complete a general framework for the design of source-problem error estimators that can be used for eigenspace error estimation. The assumptions in the framework are verified for two finite element discretizations of a model problem.

This work is organized as follows. In Section 2, we concentrate our attention on the spectral mapping theorem for rational functions of a linear operator. Section 3 is devoted to the eigenspace error estimation problem from a filtered subspace iteration. In this section, we introduce the error representation operator, which is the key to the integration of source-problem error estimators with eigenspace error estimation. In Subsections 4.1 and 4.2, we present two concrete applications of the error representation operator to the first-order system least squares (FOSLS) [12, 13] and the discontinuous Petrov-Galerkin (DPG) [25, 26, 27] discretizations of the finite element method, respectively. Both these methods, due to their nature as a residual minimization method, are able to provide intrinsic residual-based error estimators. In Section 5, we present numerical results that illustrate the performance of the proposed error estimators for a model problem.

2. RATIONAL FUNCTIONS OF AN OPERATOR

We study how the generalized eigenspaces of a rational function of a linear operator are related to those of the operator. The main result of this section is Lemma 2.1 which shows how algebraic eigenspaces are transformed by rational functions of the operator.

Let \mathcal{H} be a complex (\mathbb{C}) Hilbert space, endowed with norm $\|\cdot\|_{\mathcal{H}}$. Let $\mathcal{A} : \text{dom}(\mathcal{A}) \subseteq \mathcal{H} \rightarrow \mathcal{H}$ be a closed linear operator (that is not assumed to be bounded or selfadjoint). We use $\sigma(\cdot)$ and $\rho(\cdot)$ to denote the spectrum and resolvent set of an operator, respectively. Recall that a complex number λ in the spectrum $\sigma(\mathcal{A})$ is called an eigenvalue of \mathcal{A} if $\ker(\lambda - \mathcal{A})$ is nontrivial. Throughout, in expressions like $\lambda - \mathcal{A}$, the complex number λ also serves to denote the linear operator that scales vectors by it, and $\ker(\cdot)$ denotes the null space.

Consider complex-valued rational functions r of the form

$$r(z) = \omega_0 + \sum_{j=1}^N \sum_{i=1}^{\nu_j} \frac{\omega_{j,i}}{(z_j - z)^i} \quad (1)$$

for some $\omega_0, \omega_{j,i} \in \mathbb{C}$, some distinct $z_j \in \rho(\mathcal{A})$, and some positive integers ν_j , $j = 1, \dots, N$. Substituting z by \mathcal{A} , we define the bounded linear operator $r(\mathcal{A})$ on \mathcal{H} , namely

$$r(\mathcal{A}) = \omega_0 + \sum_{j=1}^N \sum_{i=1}^{\nu_j} \omega_{j,i} R(z_j)^i$$

where $R(z) = (z - \mathcal{A})^{-1} : \mathcal{H} \rightarrow \text{dom}(\mathcal{A})$ denotes the resolvent operator of \mathcal{A} .

A result of [66] shows that for any set of distinct complex numbers α_i and positive integers n_i , $i = 1, \dots, s$, the equality

$$\ker \left(\prod_{i=1}^s (\alpha_i - \mathcal{A})^{n_i} \right) = \bigoplus_{i=1}^s \ker(\alpha_i - \mathcal{A})^{n_i}, \quad (2)$$

holds, where the right hand side is a direct sum, when $\text{dom}(\mathcal{A}) = \mathcal{H}$. It was noted in [57] that (2) also holds when $\text{dom}(\mathcal{A})$ is smaller than \mathcal{H} and equals the domain of polynomials in \mathcal{A} of degree $d = \sum_{i=1}^s n_i$. We use this result to study how generalized eigenvectors of $r(\mathcal{A})$ are related to those of \mathcal{A} (for unbounded \mathcal{A} with general domains).

Let $\text{dom}(\mathcal{A}^1) = \text{dom}(\mathcal{A})$, and recursively define $\text{dom}(\mathcal{A}^n) = \{x \in \text{dom}(\mathcal{A}) : \mathcal{A}x \in \text{dom}(\mathcal{A}^{n-1})\}$ for any $n > 1$. Then set

$$\text{dom}(\mathcal{A}^\infty) = \bigcap_{n=1}^{\infty} \text{dom}(\mathcal{A}^n).$$

The generalized eigenspace of the unbounded \mathcal{A} corresponding to an eigenvalue λ is

$$E_\lambda^\infty(\mathcal{A}) = \bigcup_{n=1}^{\infty} \{u \in \text{dom}(\mathcal{A}^\infty) : (\mathcal{A} - \lambda)^n u = 0\}.$$

We now provide an elementary argument to relate this space to the generalized eigenspace of the bounded linear operator $r(\mathcal{A}) : \mathcal{H} \rightarrow \mathcal{H}$ corresponding to an eigenvalue $\mu \in \mathbb{C}$, namely

$$E_\mu(r(\mathcal{A})) = \bigcup_{n=1}^{\infty} \{u \in \mathcal{H} : (r(\mathcal{A}) - \mu)^n u = 0\}.$$

Let

$$r_\mu^{-1} = \{\lambda \in \mathbb{C} \setminus \{z_1, \dots, z_N\} : \mu = r(\lambda)\} \quad (3)$$

for any $0 \neq \mu \in \mathbb{C}$. This set of inverse images of μ under r is used in the next lemma.

Lemma 2.1. *For any $\mu \in \mathbb{C}$ that does not coincide with ω_0 ,*

$$E_\mu(r(\mathcal{A})) = \bigoplus_{\lambda \in r_\mu^{-1}} E_\lambda^\infty(\mathcal{A}). \quad (4)$$

Proof. Letting

$$E_\mu^\infty(r(\mathcal{A})) = \bigcup_{n=1}^{\infty} \{u \in \text{dom}(\mathcal{A}^\infty) : (r(\mathcal{A}) - \mu)^n u = 0\},$$

we claim that

$$E_\mu^\infty(r(\mathcal{A})) = E_\mu(r(\mathcal{A})). \quad (5)$$

Obviously $E_\mu^\infty(r(\mathcal{A})) \subseteq E_\mu(r(\mathcal{A}))$. To prove the reverse inclusion, we begin by proving that

$$\{u \in \mathcal{H} : (r(\mathcal{A}) - \mu)u \in \text{dom}(\mathcal{A}^\infty)\} \subseteq \text{dom}(\mathcal{A}^\infty). \quad (6)$$

Indeed, given any $u \in \mathcal{H}$, if $v = (r(\mathcal{A}) - \mu)u$ is in $\text{dom}(\mathcal{A}^\infty)$, then

$$u = \frac{1}{\omega_0 - \mu} \left(v - \sum_{j=1}^N \sum_{i=1}^{\nu_j} \omega_{j,i} R(z_j)^i u \right) \quad (7)$$

must be in $\text{dom}(\mathcal{A})$ since the $R(z_j)$ maps into $\text{dom}(\mathcal{A})$ and v is in $\text{dom}(\mathcal{A})$. Since $z_j \in \rho(\mathcal{A})$ and $u \in \text{dom}(\mathcal{A})$, the resolvent commutes with the operator when applied to u , i.e., $R(z_j)\mathcal{A}u = \mathcal{A}R(z_j)u$. Both sides of this equality are in $\text{dom} \mathcal{A}$, so repeatedly commuting, we find that $R(z_j)^i \mathcal{A}u = \mathcal{A}R(z_j)^i u$ for higher powers i as well. Hence, applying \mathcal{A} to both sides of (7),

$$\mathcal{A}u = \frac{1}{\omega_0 - \mu} \left(\mathcal{A}v - \sum_{j=1}^N \sum_{i=1}^{\nu_j} \omega_{j,i} R(z_j)^i \mathcal{A}u \right). \quad (8)$$

This shows that $\mathcal{A}u \in \text{dom}(\mathcal{A})$, i.e., $u \in \text{dom}(\mathcal{A}^2)$. Continuing this argument, we find that $u \in \text{dom}(\mathcal{A}^\infty)$, thus proving (6).

Next, observe that for any integer $k \geq 1$ and any $u \in \mathcal{H}$, if $(r(\mathcal{A}) - \mu)^k u$ is in $\text{dom}(\mathcal{A}^\infty)$, then u must also be in $\text{dom}(\mathcal{A}^\infty)$. When $k = 1$, we just proved this in (6). When $k > 1$, we use induction: since $(r(\mathcal{A}) - \mu)(r(\mathcal{A}) - \mu)^{k-1}u$ is in $\text{dom}(\mathcal{A}^\infty)$, by (6) we conclude that $(r(\mathcal{A}) - \mu)^{k-1}u$ is in $\text{dom}(\mathcal{A}^\infty)$, so by induction hypothesis, u is in $\text{dom}(\mathcal{A}^\infty)$. In particular, if $u \in \mathcal{H}$ and $(r(\mathcal{A}) - \mu)^k u = 0$, then u must be in $\text{dom}(\mathcal{A}^\infty)$. Having thus shown that $E_\mu^\infty(r(\mathcal{A})) \supseteq E_\mu(r(\mathcal{A}))$, the proof of (5) is complete.

It now suffices to prove (4) with $E_\mu(r(\mathcal{A}))$ replaced by $E_\mu^\infty(r(\mathcal{A}))$. Using polynomials

$$q(z) = \prod_{j=1}^N (z_j - z)^{\nu_j}, \quad p(z) = \sum_{j=1}^N \sum_{i=1}^{\nu_j} \omega_{j,i} \prod_{k \neq j} (z_k - z)^{\nu_k - i},$$

we may rewrite the rational function as $r(z) = p(z)/q(z)$. Then

$$r(z) - \mu = \frac{p(z) - \mu q(z)}{q(z)}. \quad (9)$$

Factorizing the numerator, we obtain finitely many distinct complex numbers λ_ℓ , $\ell = 1, \dots, L$, and associated integers n_ℓ such that

$$p(z) - \mu q(z) = \alpha \prod_{\ell=1}^L (\lambda_\ell - z)^{n_\ell} \quad (10)$$

for some scaling factor α .

Let us continue supposing that $\{\lambda_1, \dots, \lambda_L\}$ does not intersect $\{z_1, \dots, z_N\}$. (The intersecting case is dealt with at the end.) Then, from (9) and (10), it is clear that $r(z) - \mu = 0$ if and only if $z = \lambda_\ell$ for some ℓ . In other words, the inverse image of μ equals

$$r^{-1}\{\mu\} = \{\lambda_1, \dots, \lambda_L\}.$$

Let $u \in \text{dom}(\mathcal{A}^\infty)$. Since the factors of $r(\mathcal{A}) - \mu$ commute in $\text{dom}(\mathcal{A}^\infty)$,

$$(r(\mathcal{A}) - \mu)^k u = q(\mathcal{A})^{-k} \prod_{\ell} (\lambda_\ell - \mathcal{A})^{n_\ell k} u.$$

The factor $q(\mathcal{A})^{-k}$ is a composition of powers of injective resolvent operators since $z_j \in \rho(\mathcal{A})$. Hence, any $u \in \text{dom}(\mathcal{A}^\infty)$ satisfies $(r(\mathcal{A}) - \mu)^k u = 0$ if and only if

$$\prod_{\ell} (\lambda_\ell - \mathcal{A})^{n_\ell k} u = 0,$$

which, by the argument of [66] leading to (2), is equivalent to

$$u \in \bigoplus_{\ell=1}^L \ker(\lambda_\ell - \mathcal{A})^{n_\ell k}.$$

This proves that

$$E_\mu^\infty(r(\mathcal{A})) = \bigoplus_{\lambda \in r^{-1}\{\mu\}} E_\lambda^\infty(\mathcal{A}) \quad (11)$$

holds for the current case.

To finish the proof, consider the postponed case where there are integers ℓ and i such that $\lambda_\ell = z_i$. If $n_\ell \leq \nu_i$, then we may cancel off the common factor $(z_i - z)^{n_\ell}$ from the numerator and denominator of (9) and reuse the above arguments with $\tilde{q}(z) = q(z)/(z_i - z)^{n_\ell}$, a polynomial of lower degree, in place of $q(z)$. Then, $r^{-1}\{\mu\}$ no longer contains the associated λ_ℓ , so λ_ℓ no longer contributes to the sum of (11). If $n_\ell > \nu_i$, then the numerator in (9) will still contain a factor of $\lambda_\ell - z$, so $r^{-1}\{\mu\}$ continues to contain λ_ℓ . But $E_{\lambda_\ell}(\mathcal{A})$ is trivial, since $\lambda_\ell = z_i$ is in the resolvent set of \mathcal{A} . Hence it only contributes the trivial space to the sum in (11) and can be removed from the sum. \square

Example 2.2 (A finite-dimensional case). Consider a linear operator \mathcal{A} on $\mathcal{H} = \mathbb{C}^3$ represented by the matrix

$$\mathcal{A} = \begin{bmatrix} -\frac{1}{2} & 0 & 0 \\ 0 & \frac{1}{2} & 1 \\ 0 & 0 & \frac{1}{2} \end{bmatrix}$$

in Jordan canonical form. Here, abusing notation, we have identified the linear operator with its matrix representation obtained using the standard unit basis vectors denoted by e_1, e_2 , and e_3 . The eigenvalues of \mathcal{A} are $-\frac{1}{2}$ and $\frac{1}{2}$, with algebraic multiplicities 1 and 2,

respectively. Their generalized eigenspaces are $E_{-1/2}^\infty = \text{span}(e_1)$ and $E_{1/2}^\infty = \text{span}(e_2, e_3)$. Define the rational function

$$r(z) = -\frac{1}{z^2 + 1} = \frac{i}{2(z - i)} + \frac{-i}{2(z + i)}. \quad (12)$$

It is immediately verified that the image of all eigenvalues of \mathcal{A} under r equal $-\frac{4}{5}$. In particular, the inverse image r_μ^{-1} of $\mu = -\frac{4}{5}$ equals

$$r_{-4/5}^{-1} = \left\{ \frac{1}{2}, -\frac{1}{2} \right\}, \quad (13)$$

the entire spectrum of \mathcal{A} . Functions of Jordan forms are easy to compute and in this case we obtain

$$r(\mathcal{A}) = \begin{bmatrix} -\frac{4}{5} & 0 & 0 \\ 0 & -\frac{4}{5} & \frac{16}{25} \\ 0 & 0 & -\frac{4}{5} \end{bmatrix}.$$

In particular, it shows that the generalized eigenspace of the eigenvalue $-4/5$ is the entire space \mathbb{C}^3 . This eigenspace also admits the direct decomposition

$$\begin{aligned} E_{-4/5}(r(\mathcal{A})) &= \mathbb{C}^3 = \text{span}(e_1) \oplus \text{span}(e_2, e_3) \\ &= E_{-1/2}^\infty(\mathcal{A}) \oplus E_{1/2}^\infty(\mathcal{A}), \end{aligned}$$

thus illustrating the identity of Lemma 2.1 in a simple finite-dimensional case.

Example 2.3 (The Cayley transform of an operator). Consider the Cayley transform

$$r(z) = \frac{z - i}{z + i} = 1 - \frac{2i}{z + i}, \quad (14)$$

which maps the upper half-plane to the unit disk [43, Theorem 6.3.6]. This is a Möbius transform (or a linear fractional transformation), see e.g., [23, Section III.3] or [43, Section 6.3]. In this example, we set the linear operator \mathcal{A} on $\mathcal{H} = \mathbb{C}^3$ as represented by the matrix in Jordan canonical form

$$\mathcal{A} = \begin{bmatrix} 10 - i & 0 & 0 \\ 0 & 10 + i & 1 \\ 0 & 0 & 10 + i \end{bmatrix},$$

whose eigenvalues are $10 - i$ and $10 + i$, with algebraic multiplicities 1 and 2, respectively. The image of these eigenvalues under the Cayley transform r defined in (14) are $r(10 - i) = \frac{5-i}{5}$ and $r(10 + i) = \frac{25-5i}{26}$. As Möbius transforms are invertible, the inverse images r_μ^{-1} , for $\mu_1 = \frac{5-i}{5}$ and $\mu_2 = \frac{25-5i}{26}$ are singletons. The Cayley transform of \mathcal{A} is

$$r(\mathcal{A}) = \begin{bmatrix} \mu_1 & 0 & 0 \\ 0 & \mu_2 & \frac{5+50i}{676} \\ 0 & 0 & \mu_2 \end{bmatrix},$$

whose eigenvalues are μ_1 and μ_2 , with algebraic multiplicities 1 and 2, respectively. It can be checked readily that the generalized eigenspaces of $r(\mathcal{A})$ satisfy the identity of Lemma 2.1.

It is worth noting that $|\mu_1| = \sqrt{26}/5 > 1$ and $|\mu_2| = 5/\sqrt{26} < 1$, which is consistent with the mapping properties of the Cayley transform. This example illustrates how Möbius transforms can be used to map some parts of the spectrum of an operator into dominant eigenvalues (larger in absolute value than the rest of the spectrum) of the transformed operator.

Remark 2.4 (General rational functions). A general rational function is a quotient of two polynomials $p(z)$ and $q(z)$ over the complex field, namely, $r(z) = p(z)/q(z)$. It is well-known (see, e.g., [23, Eq. V.1.9] or [54, Theorems IV.5.2–IV.5.3]) that we can express r in a partial fraction expansion: denoting the zeros of $q(z)$ by z_i , with multiplicity ν_i , there exist coefficients $\omega_{j,i} \in \mathbb{C}$ and a polynomial $\hbar(z)$ representing the holomorphic part of r , such that

$$r(z) = \hbar(z) + \mathfrak{s}(z), \quad \text{where} \quad \mathfrak{s}(z) = \sum_{j=1}^N \sum_{i=1}^{\nu_j} \frac{\omega_{j,i}}{(z_j - z)^i}. \quad (15)$$

As before, assume that $z_j \in \rho(\mathcal{A})$. Then, the proof of Lemma 2.1 can be generalized to this case to show that *for any $\mu \in \mathbb{C}$ such that*

$$\hbar_\mu^{-1} \cap \sigma(\mathcal{A}) = \emptyset, \quad (16)$$

the equality (4) continues to hold for the $r(z)$ in (15). Here $\hbar_\mu^{-1} := \{z \in \mathbb{C} : \hbar(z) = \mu\}$ denotes the set of zeros of $\hbar(z) - \mu$. The change in the proof needed to achieve this generalization involves replacing (7) by

$$u = (\hbar(\mathcal{A}) - \mu)^{-1} (v - \mathfrak{s}(\mathcal{A})u),$$

where the inverse exists and can be written as a composition of resolvents due to (16) and the fundamental theorem of algebra. This proves that u is in $\text{dom}(\mathcal{A})$ whenever v is in $\text{dom}(\mathcal{A})$, and iterating, one establishes (6), (5), and the remainder of proof of the lemma as before. Note that condition (16) generalizes the condition $\mu \neq \omega_0$ of Lemma 2.1: indeed, when $\hbar(z) = \omega_0$, a polynomial of degree zero, $\mu \neq \omega_0$ implies that $\hbar_\mu^{-1} = \emptyset$ so (16) holds.

3. ESTIMATING THE ERROR IN EIGENSPACE

Often, in practical problems, the need arises to numerically approximate the eigenspace corresponding to a finite cluster of eigenvalues in $\sigma(\mathcal{A})$. Here, “cluster” refers to a finite set of eigenvalues that are relatively close to each other and well separated from the rest of the spectrum. The main result of this section, Theorem 3.10, provides a computable reliable eigenspace error estimator under suitable assumptions.

Recall that an eigenvalue is called an isolated eigenvalue if it has an open neighborhood in \mathbb{C} whose all other points belong to $\rho(\mathcal{A})$. Let Λ denote a finite set of isolated eigenvalues of \mathcal{A} . Let $m(\lambda, \mathcal{A})$ denote the algebraic multiplicity of λ as an eigenvalue of \mathcal{A} . For all $z \in \rho(\mathcal{A})$, we set $m(z, \mathcal{A}) = 0$. Henceforth, we assume that $m(\lambda, \mathcal{A}) < \infty$ for each eigenvalue λ in the cluster Λ .

We are interested in controlling the error in approximation of the algebraic eigenspace E of the cluster of eigenvalues Λ . Let the set Λ be enclosed within Γ , a positively oriented, bounded, simple, closed contour that lies entirely in $\rho(\mathcal{A})$ and encloses no element of $\sigma(\mathcal{A})$ other than those in Λ . Then the Riesz projector associated to the cluster Λ is

$$S = \frac{1}{2\pi i} \oint_{\Gamma} R(z) dz. \quad (17)$$

Hence the wanted eigenspace is the range of S ,

$$E = \text{ran } S \subset \text{dom}(\mathcal{A}),$$

and

$$\dim E = \sum_{\lambda \in \Lambda} m(\lambda, \mathcal{A}) < \infty.$$

Before approximating E , we map the cluster using rational functions of the form (1), restricted further, for simplicity, to the form

$$r(z) = \omega_0 + \sum_{j=1}^N \frac{\omega_j}{z_j - z} \quad (18)$$

for some $\omega_j \in \mathbb{C}$. To mimic the behavior of the operator-valued integral (17), it usually suffices to consider rational functions of the restricted form (18) (as will be clear from Example 3.6 later). The set Λ is mapped by r to

$$\Upsilon = \{r(\lambda) : \lambda \in \Lambda\}. \quad (19)$$

Let

$$S_r = r(\mathcal{A}) = \omega_0 + \sum_{j=1}^N \omega_j R(z_j). \quad (20)$$

Many algorithmic techniques construct specific rational functions r of interest that make Υ more easily capturable than Λ , e.g., rational functions r that make Υ into a set of “dominant eigenvalues” of S_r easily captured by power iterations. Postponing discussion of such details, we proceed making the following assumption.

Assumption 3.1 (On Rational Functions). Assume that r is of the form (18),

$$\omega_0 \notin \Upsilon \quad \text{and} \quad \bigcup_{\mu \in \Upsilon} r_\mu^{-1} \cap \sigma(\mathcal{A}) \subseteq \Lambda \quad (21)$$

where r_μ^{-1} is as defined in (3) and Υ is as in (19).

Let Θ a simple closed curve in the complex plane enclosing Υ and not enclosing the origin nor any point of $\sigma(S_r) \setminus \Upsilon$. Define

$$\begin{aligned} P_r &= \frac{1}{2\pi i} \oint_{\Theta} (z - S_r)^{-1} dz, \\ E_r &= \text{ran } P_r. \end{aligned}$$

Lemma 3.2. *Suppose Assumption 3.1 holds. Then every $\mu \in \Upsilon$ is an eigenvalue of S_r of algebraic multiplicity*

$$m(\mu, S_r) = \sum_{\lambda \in r_\mu^{-1}} m(\lambda, \mathcal{A}). \quad (22)$$

Moreover, the spaces E_r and E coincide.

Proof. Let $\mu \in \Upsilon$. By (21), $\mu \neq \omega_0$. Hence, Lemma 2.1 applies and (4) holds. By counting dimensions on both sides of (4), the stated equality (22) follows.

Clearly, μ is an eigenvalue of S_r if and only if its algebraic eigenspace $E_\mu(S_r)$ is nontrivial. The equality (4) implies that the eigenspace $E_\mu(S_r)$ is nontrivial if and only if there is a λ in r_μ^{-1} such that $E_\lambda^\infty(\mathcal{A})$ is nontrivial, i.e., if and only if there is a λ in $r_\mu^{-1} \cap \sigma(\mathcal{A})$. Since $r_\mu^{-1} \cap \sigma(\mathcal{A})$ is contained in Λ by (21) of Assumption 3.1, the equality (4) implies the sum of the eigenspaces of all μ in Υ satisfies

$$\sum_{\mu \in \Upsilon} E_\mu(r(\mathcal{A})) = \sum_{\mu \in \Upsilon} \bigoplus_{\lambda \in r_\mu^{-1} \cap \sigma(\mathcal{A})} E_\lambda^\infty(\mathcal{A}) = \sum_{\lambda \in \Lambda} E_\lambda^\infty(\mathcal{A}).$$

The left and right hand sides equal E_r and E , respectively, so $E_r = E$. \square

Example 3.3. Reviewing the case of the $r(z)$ and \mathcal{A} of Example 2.2, putting $\Lambda = \{-1/2, 1/2\}$, we have $\Upsilon = \{-4/5\}$ (which clearly does not contain $\omega_0 = 0$). Then (13) shows that Assumption 3.1 holds.

Example 3.4 (The Cayley transform revisited). Reviewing the case of the Cayley transform $r(z)$ and \mathcal{A} of Example 2.3, putting $\Lambda = \{10 - i, 10 + i\}$, we have $\Upsilon = \{(5 - i)/5, (25 - 5i)/26\}$. Clearly $\omega_0 = 1$ for this $r(z)$, which is not in contained in Υ , so the first condition in (21) holds. The second condition in (21) also holds since the inverse images of the two elements of Υ are exactly the two eigenvalues in Λ .

Example 3.5 (Rational function in inverse iterations). When a single isolated eigenvalue $\lambda_1 \in \mathbb{C}$ of a linear operator \mathcal{A} on \mathcal{H} is to be targeted, the cluster $\Lambda = \{\lambda_1\}$ is a singleton. A standard approach in this case is to perform an inverse iteration to capture the eigenspace of λ_1 . This iteration consists of repeated application of powers of $r(\mathcal{A})$ on some initial subspace for an r of the form

$$r(z) = \frac{1}{z_1 - z},$$

using a “guess” $z_1 \in \mathbb{C}$ that is close but not equal to λ_1 . In this case the nonzero complex number $\mu = r(\lambda_1) = (z_1 - \lambda_1)^{-1}$ is the only element of Υ . We also immediately see that $\mu = r(\lambda)$ if and only if $\lambda = \lambda_1$, i.e., $r_\mu^{-1} = \Lambda$. Clearly Assumption 3.1 holds in this case.

Example 3.6 (A rational function in FEAST iterations). The so-called “FEAST” contour integral eigensolver [61, 38] uses rational functions obtained by replacing the contour integral over Γ in (17) by a quadrature. Consider the case of a circular contour Γ centered at some $O \in \mathbb{C}$ of radius $R > 0$, parameterized by $O + R\phi e^{i\theta}$ with some initial phase factor ϕ of unit magnitude. Rewriting the contour integral over Γ as an integral over $[0, 2\pi]$ based on this parameterization, and applying the trapezoidal rule with N points, we obtain a rational function of the form (1) with

$$\omega_j = \widehat{\omega}_N^{j-1} R\phi/N, \quad z_j = R\phi \widehat{\omega}_N^{j-1} + O \quad (23)$$

where $\widehat{\omega}_N = e^{i2\pi/N}$. A commonly made choice is $\phi = \pm e^{i\pi/N}$. (The case $N = 2$ with $O = 0$ and $R = 1$ yields (12) in Example 2.2.) Such rational functions are often known as “Butterworth filters” in signal processing [47]. Note that the powers of $\widehat{\omega}_N$ appearing above, namely $\widehat{\omega}_N^j$ for $j = 0, \dots, N-1$, are the N th roots of unity. By a partial fraction expansion (see [38, Example 2.2]) one can show that with the settings in (23), we have

$$r(z) = \sum_{j=1}^N \frac{\omega_j}{z_j - z} = \left[1 - \left(\frac{z - O}{R\phi} \right)^N \right]^{-1}. \quad (24)$$

Let $D = \{z \in \mathbb{C} : |z - O| < R\}$ be the disk enclosed by Γ . Now suppose we are in the setting described in the beginning of this section, where we have an eigenvalue cluster of interest Λ that lies in D and

$$\sigma(\mathcal{A}) \cap D = \Lambda. \quad (25)$$

Then we claim that Assumption 3.1 holds. Indeed, since $|z - O| < |R\phi|$, the second expression for $r(z)$ in (24) and triangle inequality yields

$$|r(z)| > \frac{1}{2} \quad \text{for all } z \in D.$$

Hence none of the elements of \mathcal{Y} can equal $\omega_0 = 0$. Next, consider any $\mu \in \mathcal{Y}$. There must be a $\lambda \in \Lambda$ such that $\mu = r(\lambda)$. Any z in r_μ^{-1} must therefore satisfy $r(z) = r(\lambda)$, or equivalently $(z - O)^N = (\lambda - O)^N$. Hence z must equal one of the complex numbers

$$\zeta_\ell = O + (\lambda - O) \widehat{\omega}_N^\ell, \quad \ell = 0, \dots, N-1,$$

all of which lie in D , i.e., we have shown that $r_\mu^{-1} = \{\zeta_\ell : \ell = 0, \dots, N-1\} \subset D$. By (25), the only elements of the spectrum of \mathcal{A} in D are those in Λ , so it follows that $r_\mu^{-1} \cap \sigma(\mathcal{A}) \subseteq \Lambda$, thus verifying (21).

Next, we proceed to approximate S_r and study how the eigenspaces change under such approximations. Throughout we suppose there is a Hilbert space V , normed by $\|\cdot\|_V$, that is continuously embedded into \mathcal{H} such that $\text{dom}(\mathcal{A}) \subseteq V$. Typical examples of V include the whole space \mathcal{H} , or the set $\text{dom}(\mathcal{A})$ after making into a Hilbert space using the graph norm of \mathcal{A} , or the domain of the a sesquilinear form from which \mathcal{A} arises. Such examples were discussed in [38], where the next assumption can also be found.

Assumption 3.7 (On Resolvent Approximations). We assume that there are finite-dimensional subspaces $V_h \subset V$ (indexed by a discretization parameter h approaching zero) and finite-rank operators $R_h(z) : \mathcal{H} \rightarrow V_h$ such that

$$\lim_{h \rightarrow 0} \|R_h(z_k) - R(z_k)\|_V = 0 \quad (26)$$

for every $k = 1, \dots, N$.

Under this assumption, the operator

$$S_{r,h} = \omega_0 + \sum_{j=1}^N \omega_j R_h(z_j) \quad (27)$$

is an approximation of S_r . Note that Assumption 3.7, in particular, restricts us to consider only operators \mathcal{A} with compact resolvent (since V_h is finite dimensional). Equation (26) allows us to define a natural approximate eigenspace as follows. It implies that $\|S_{r,h} - S_r\|_V$ converges to 0 as h approaches 0. Hence, given any open disc enclosing a single isolated eigenvalue $\mu \in \mathcal{Y}$ of S_r , for sufficiently small h , there are exactly as many eigenvalues of $S_{r,h}$ in the same disc as the algebraic multiplicity $m(\mu, S_r)$. In particular, this implies that, for sufficiently small h , the contour Θ is in the resolvent set of $S_{r,h}$ and encloses as many eigenvalues of joint multiplicity equal to $\dim E_r$. Hence, the integral

$$P_{r,h} = \frac{1}{2\pi i} \oint_{\Theta} (z - S_{r,h})^{-1} dz$$

is well defined and its range

$$E_h = \text{ran } P_{r,h} \quad (28)$$

has the same dimension as the space E_r it intends to approximate:

$$\dim E_h = \dim E_r. \quad (29)$$

We tacitly assume throughout that h has been made small enough for (29) to hold and for the above definitions to make sense. In practice, one computes (a basis for) the approximate eigenspace E_h in (28) through subspace iterations—see, e.g., [38, Theorem 3.4] which shows how certain subspace iterates approach E_h , or see Section 5, where we use a subspace iteration based on operator-valued contour integrals to compute E_h .

Comparison of the spaces E and E_h is done through the gap metric in V . To define it, first let

$$\delta(U, W) = \sup_{u \in U, \|u\|_V=1} \text{dist}_V(u, W) = \|(I - Q_W)Q_U\|_V$$

for any two closed subspaces U and W of V . Here $\text{dist}_V(u, V) = \inf_{v \in V} \|u - v\|_V$, I denotes the identity on V , and Q_W denotes the V -orthogonal projection into W . Symmetrizing this, we define the gap by

$$\text{gap}_V(U, W) = \max \left(\delta(U, W), \delta(W, U) \right).$$

The argument of the next lemma is similar to the proof of [38, Theorem 4.1], but the key difference is that the supremum appearing in Lemma 3.8 is taken over the approximating space E_h , not the exact eigenspace E .

Lemma 3.8. *If Assumption 3.7 holds, then there exist $C_r > 0$ and $h_0 > 0$ such that for all $h < h_0$,*

$$\text{gap}_V(E_r, E_h) \leq C_r \sup_{e_h \in E_h, \|e_h\|_V=1} \|(S_r - S_{r,h})e_h\|_V. \quad (30)$$

Proof. We begin by noting that

$$\begin{aligned} P_r - P_{r,h} &= \frac{1}{2\pi i} \oint_{\Theta} \left[(z - S_r)^{-1} - (z - S_{r,h})^{-1} \right] dz \\ &= \frac{1}{2\pi i} \oint_{\Theta} (z - S_r)^{-1} [S_r - S_{r,h}] (z - S_{r,h})^{-1} dz. \end{aligned}$$

Since generalized eigenspaces of any operator are invariant subspaces of its resolvent,

$$(z - S_{r,h})^{-1} E_h \subseteq E_h.$$

Consequently, for any $e_h \in E_h$, we have

$$\begin{aligned} \|(P_{r,h} - P_r)e_h\|_V &= \frac{1}{2\pi} \left\| \oint_{\Theta} (z - S_r)^{-1} (S_r - S_{r,h}) Q_{E_h} (z - S_{r,h})^{-1} e_h dz \right\| \\ &\leq \left(\frac{1}{2\pi} \oint_{\Theta} \|(z - S_r)^{-1}\|_V \|(z - S_{r,h})^{-1}\|_V dz \right) \|(S_r - S_{r,h}) Q_{E_h}\|_V \|e_h\|_V \end{aligned}$$

Bound the term within parentheses above by C_r and note that we may choose such a bound independently of h when h is sufficiently small due to (26) of Assumption 3.7. We use the above estimate to conclude that

$$\begin{aligned} \delta(E_h, E_r) &= \sup_{e_h \in E_h, \|e_h\|_V=1} \text{dist}_V(e_h, E_r) \\ &\leq \sup_{e_h \in E_h, \|e_h\|_V=1} \|e_h - P_r e_h\|_V \\ &= \sup_{e_h \in E_h, \|e_h\|_V=1} \|(P_{r,h} - P_r)e_h\|_V \\ &\leq C_r \|(S_r - S_{r,h}) Q_{E_h}\|_V. \end{aligned} \quad (31)$$

This implies, by (26), that there is an $h_0 > 0$ such that $\delta(E_h, E_r) = \|(I - Q_{E_r})Q_{E_h}\|_V < 1$ for all $h < h_0$. Then the two alternatives of [51, Theorem I.6.34] apply: they imply that there is a subspace $\tilde{E}_r \subseteq E_r$ such that

$$\delta(E_h, E_r) = \delta(E_h, \tilde{E}_r) = \text{gap}(E_h, \tilde{E}_r) < 1. \quad (32)$$

Note that

$$\begin{aligned}\dim \tilde{E}_r &= \dim E_h && \text{by (32)} \\ &= \dim E_r && \text{by (29).}\end{aligned}$$

Since $\tilde{E}_r \subseteq E_r$, this implies that $E_r = \tilde{E}_r$. Hence $\text{gap}(E_h, \tilde{E}_r) = \text{gap}(E_h, E_r)$, which by (32) also equals $\delta(E_h, E_r)$. Therefore, (31) shows that $\text{gap}(E_h, \tilde{E}_r) = \text{gap}(E_h, E_r) = \delta(E_h, E_r) \leq C_r \| (S_r - S_{r,h}) Q_{E_h} \|_V$, proving the result. \square

The lemma now leads to our main result, which produces an error estimator for the gap between the true and the approximate eigenspace by suitably combining error estimators for certain linear source problems. Suppose there is a Hilbert space Y , with norm $\| \cdot \|_Y$, into which such error estimators for source problems can be computed—they are denoted by \mathcal{E} in the next assumption.

Assumption 3.9 (On Source Error Estimators). There is a $C_0 > 0$ and a linear operator $\mathcal{E} : V_h \rightarrow Y$ (whose application to any $v \in V_h$ is easily computable) satisfying

$$\| S_r v_h - S_{r,h} v_h \|_V \leq C_0 \| \mathcal{E} v_h \|_Y, \quad v_h \in V_h. \quad (33)$$

To understand the relevance of this assumption, subtract (27) from (20) to get

$$S_r v_h - S_{r,h} v_h = \sum_{j=1}^N \omega_j (R(z_j) v_h - R_h(z_j) v_h).$$

Each summand above can be estimated by observing that $u_h = R_h(z_j) v_h$ is an approximation to the solution u of the source problem $(z - \mathcal{A})u = v_h$. This is why we referred to \mathcal{E} as an error estimator from source problems.

Our goal is to repurpose such source problem error estimators to estimate the error in the eigenspace approximation E_h . Assuming that a basis e_h^i , $i = 1, \dots, L$, for the eigenspace approximation E_h has been computed, we define the $L \times L$ matrices

$$G_{ij} = (\mathcal{E} e_h^j, \mathcal{E} e_h^i)_Y, \quad M_{ij} = (e_h^j, e_h^i)_V \quad (34)$$

using the inner products of Y and V , respectively. Consider the small $L \times L$ Hermitian generalized eigenproblem $Gx = \lambda Mx$. Let its maximal eigenvalue be denoted by $\hat{\lambda}$, i.e.,

$$\hat{\lambda} = \max \sigma(M^{-1}G),$$

and let \hat{x} denote an eigenvector of eigenvalue $\hat{\lambda}$. Let

$$\tilde{e}_h = \sum_{i=1}^L \hat{x}_i e_h^i, \quad \hat{e}_h = \frac{\tilde{e}_h}{\|\tilde{e}_h\|_V}. \quad (35)$$

The latter function in E_h serves as an eigenspace error indicator after an application of \mathcal{E} , whose global reliability is proved next. The proof also makes it clear that \hat{e}_h does not depend on the specific choice of e_h^j but only on the space E_h .

Theorem 3.10 (Eigenspace Gap Estimator). *Suppose Assumptions 3.1, 3.7 and 3.9 hold. Then, there is an $h_0 > 0$ and $C > 0$ such that for all $h < h_0$,*

$$\text{gap}_V(E_h, E) \leq C \| \mathcal{E} \hat{e}_h \|_Y$$

where the estimator $\mathcal{E} \hat{e}_h$ is computed using (only) the approximate eigenspace E_h .

Proof. Since Assumption 3.1 holds, by Lemma 3.2, we have $E = E_r$. Hence verifying the conditions of Lemma 3.8 (by virtue of the remaining two assumptions), its estimate (30) implies

$$\begin{aligned} \text{gap}_V(E, E_h) &= \text{gap}_V(E_r, E_h) \leq C_r \sup_{e_h \in E_h, \|e_h\|_V=1} \|(S_r - S_{r,h})e_h\|_V \\ &\leq C_r C_0 \sup_{e_h \in E_h} \frac{\|\mathcal{E}e_h\|_Y}{\|e_h\|_V}. \end{aligned} \quad (36)$$

Writing any $e_h \in E_h$ as $e_h = \sum_{i=1}^L x_i e_h^i$, we find that

$$\frac{\|\mathcal{E}e_h\|_Y^2}{\|e_h\|_V^2} = \frac{x^* G x}{x^* M x},$$

which is the Rayleigh quotient of the eigenproblem $Gx = \lambda Mx$. It is maximized by an eigenvector \hat{x} of its maximal eigenvalue $\hat{\lambda}$. Hence the supremum in (36) is attained by \hat{e}_h of (35) and the result follows with $C = C_r C_0$. \square

We conclude this section with a discussion of Theorem 3.10, a result useful for adaptive algorithms for eigenvalue clusters. As seen from the above proof, the computable source estimator $\mathcal{E}\hat{e}_h$ depends only on the computed eigenspace E_h , and not on individual eigenvectors within it. In this sense, our estimator is cluster robust. Computing a supremum over a finite dimensional approximate space for error estimation, as used in the above proof, is a technique that can also be found in other works, e.g., in [56], where the authors develop estimates of gap between exact and approximate eigenspaces of a generalized selfadjoint eigenvalue problem. The idea of using source problem error estimates for eigenvalue adaptivity can also be found in the works of [45, 4, 34, 33], where residuals generated by solution operators, applied to approximate eigenfunctions, feature prominently. Such residuals are then further estimated by using an auxiliary space (e.g., appropriate bubble spaces in the finite element context), which then provide control of relative eigenvalue errors. Specific new examples of locally computable \mathcal{E} for a selfadjoint problem appear in the next section (Section 4) and a nonselfadjoint example can be found in Section 5.

4. APPLICATION TO FINITE ELEMENT DISCRETIZATIONS

In this section, we apply the framework for eigenspace error estimators we developed in Section 3, specifically Theorem 3.10, to some finite element examples. We illustrate how to verify Assumptions 3.7 and 3.9 for a typical partial differential operator. (Verification of the only other assumption in the theorem, namely Assumption 3.1, was already illustrated in prior examples—see for instance Example 3.6.)

Throughout this section, we set

$$\mathcal{H} = L^2(\Omega), \quad V = \mathring{H}^1(\Omega), \quad \mathcal{A} = -\Delta,$$

with $\text{dom}(\mathcal{A}) = \{u \in V : \Delta u \in L_2(\Omega)\}$. Here Ω is a Lipschitz polygonal subset of \mathbb{R}^2 and we have used standard notation for Sobolev spaces, e.g., the space $L^2(\Omega)$ denotes the Hilbert space of square-integrable functions on Ω endowed with the standard inner product, and $\mathring{H}^1(\Omega)$ denote its Sobolev subspace functions with square-integrable weak derivatives and vanishing trace on the boundary $\partial\Omega$. Our interest is in approximating eigenspaces of some targeted eigenvalue clusters of \mathcal{A} .

Given any $f \in \mathcal{H}$, the application of the resolvent at a $z \in \rho(\mathcal{A})$ produces $u = R(z)f$ that solves the Dirichlet problem

$$zu + \Delta u = f \quad \text{in } \Omega, \quad u = 0 \quad \text{on } \partial\Omega. \quad (37)$$

Its weak formulation is to find $u \in \mathring{H}^1(\Omega)$ satisfying

$$b_z(u, v) = (f, v)_{L^2}, \quad \text{for all } v \in \mathring{H}^1(\Omega), \quad (38)$$

where the sesquilinear form b_z is defined by

$$b_z(u, v) = z(u, v)_{L^2} - (\nabla u, \nabla v)_{L^2} \quad (39)$$

for any $u, v \in \mathring{H}^1(\Omega)$. Here and throughout, $(\cdot, \cdot)_{L^2}$ and $\|\cdot\|_{L^2}$ denote the inner product and norm, respectively, on $L^2(\Omega)$ or its Cartesian products. The inf-sup condition holds for $b_z(\cdot, \cdot)$ as shown in [39, Lemma 3.1], i.e.,

$$\sup_{v \in \mathring{H}^1(\Omega)} \frac{b_z(w, v)}{\|\nabla v\|_{L^2}} \geq \frac{1}{\beta_z} \|\nabla w\|_{L^2}, \quad (40)$$

holds for all $w \in \mathring{H}^1(\Omega)$ with $\beta_z = \sup_{\lambda \in \sigma(\mathcal{A})} \left| \frac{\lambda}{\lambda - z} \right|$. Moreover, by our assumption on the boundary of Ω , it consists of smooth segments intersecting at finitely many vertices and there is some $1/2 < \alpha$ such the largest interior angle subtended at such vertices is π/α . Then for any $s < \alpha$, standard elliptic regularity theory [44] shows that there is a constant $C_{z,\text{reg}} > 0$ such that

$$\|R(z)f\|_{H^{1+s}(\Omega)} \leq C_{z,\text{reg}} \|f\|_{\mathcal{H}}, \quad \text{for all } f \in \mathcal{H} \text{ and } z \in \rho(\mathcal{A}). \quad (41)$$

This gives the stability of solutions of (38). Note that $V = \mathring{H}^1(\Omega)$ is endowed with the $H^1(\Omega)$ -norm, so it is continuously embedded into \mathcal{H} , since $\|u\|_{\mathcal{H}} = \|u\|_{L_2} \leq \|u\|_{H^1(\Omega)}$ for all $u \in V$. Moreover, $R(z)V \subset V$ for all $z \in \rho(\mathcal{A})$, since $\text{dom}(\mathcal{A})$ is contained in V in this example.

We now proceed to discuss discretization by FOSLS (First-Order Systems Least Squares) and DPG (Discontinuous Petrov-Galerkin) methods. The FOSLS method was developed in [12, 13] and a detailed account of its development can be found in the book [8]. The DPG method and its error estimators were developed in [24, 28, 16] and a recent review [27] summarizes these developments. In both cases, we use Ω_h , a conformal simplicial finite element mesh of Ω , that is decomposed into different elements K . Given $K \subset \Omega$ and an integer $k \geq 0$, we denote by $P^k(K)$ the space of polynomials of degree at most k defined on K , and by $P_{\mathcal{H}}^k(K)$ the space of homogeneous polynomials of degree k defined on K . The local Raviart-Thomas space on an element K equals $RT^k(K) = P^k(K)^d \oplus P_{\mathcal{H}}^k(K)x$, where $x = (x_1, \dots, x_d)$ is the position vector in K . We adopt the convention of writing $B_1 \lesssim B_2$ whenever the inequality $B_1 \leq CB_2$ holds with some mesh-independent constant C whose value at different occurrences may differ.

4.1. Eigenspace error estimation using FOSLS estimators. The FOSLS discretization of the resolvent operator of \mathcal{A} starts with a first-order reformulation of (37) by introducing the flux $q = -\nabla u$. Let $X := H(\text{div}) \times \mathring{H}^1(\Omega)$. Then defining the first-order operator $A_z : X \rightarrow L_2(\Omega)^2 \times L_2(\Omega)$ by

$$A_z(q, u) = (q + \nabla u, -\text{div } q + zu)$$

the resolvent problem (37) takes the form

$$(q, u) \in X : \quad A_z(q, u) = (0, f), \quad (42)$$

for any $f \in \mathcal{H}$. This identifies, in addition to $R(z)f$, a mapping into the flux component, which we denote by $R^q(z)f$, i.e.,

$$f \xrightarrow{R(z)} u \text{ solving (42)}, \quad f \xrightarrow{R^q(z)} q \text{ solving (42)}.$$

For any integer $k \geq 1$, consider the Lagrange and the Raviart-Thomas finite element spaces given by

$$V_h = \left\{ v \in \mathring{H}^1(\Omega) : v|_K \in P^k(K), \text{ for all } K \in \Omega_h \right\},$$

$$RT_h = \left\{ q \in H(\text{div}, \Omega) : q|_K \in RT^{k-1}(K), \text{ for all } K \in \Omega_h \right\},$$

respectively (see, e.g., [32, 11]) and put $X_h = RT_h \times V_h$.

The two ingredients needed in our framework, namely $R_h(z)$ and \mathcal{E} , are now set as follows. Set the approximate resolvent operator $R_h(z) : \mathcal{H} \rightarrow V_h$ as the second component of the unique $(q_h, u_h) \in X_h$ that solves the FOSLS equation

$$(A_z(q_h, u_h), A_z(r_h, v_h))_{L_2} = ((0, f), A_z(r_h, v_h))_{L_2}, \quad (43)$$

for all $(r_h, v_h) \in X_h$, i.e., $R_h(z)f := u_h$. Let us also denote the flux component of the solution by $R_h^q(z)f := q_h$, i.e.,

$$f \xrightarrow{R_h(z)} u_h \text{ solving (43)}, \quad f \xrightarrow{R_h^q(z)} q_h \text{ solving (43)}.$$

Next, to define the error estimator $\mathcal{E} : V_h \rightarrow Y$, setting $Y = [L_2(\Omega)^2 \times L_2(\Omega)]^N$, we consider, for each pole z_k of the rational function in (1), an operator $\mathcal{E}_k : V_h \rightarrow L_2(\Omega)^2 \times L_2(\Omega)$ defined by

$$\mathcal{E}_k v_h = (0, v_h) - A_{z_k}(R_h^q(z_k)v_h, R_h(z_k)v_h) \quad (44a)$$

for any $v_h \in V_h$ and set

$$\mathcal{E} v_h = (\mathcal{E}_1 v_h, \dots, \mathcal{E}_N v_h) \in Y. \quad (44b)$$

Note that $\|\mathcal{E} v_h\|_Y^2 = \sum_{k=1}^N \|\mathcal{E}_k v_h\|_{L_2}^2$. With these definitions in place, we now proceed to verify Assumptions 3.7 and 3.9.

Lemma 4.1. *For any $z \in \rho(\mathcal{A})$, there exists $\gamma_z > 0$ such that, for all $u \in \mathring{H}^1(\Omega)$ and $q \in H(\text{div})$, we have*

$$\|q\|_{L_2}^2 + \|u\|_{H^1(\Omega)}^2 \leq \gamma_z \|A_z(q, u)\|_{L_2}^2. \quad (45)$$

Moreover, the operator A_z is a continuous bijection.

Proof. Let $u \in \mathring{H}^1(\Omega)$ and $q \in H(\text{div})$ and let $g \in L_2(\Omega)^2$ and $f \in L_2(\Omega)$ be such that $A_z(q, u) = (g, f)$. This is a system of two equations, from which eliminating q , we obtain $zu - \text{div}(g - \nabla u) = f$. Rearranging,

$$(z + \Delta)u = f + \text{div } g,$$

which, due to the boundary condition on u , has the following associated weak formulation

$$b_z(u, v) = (f + \text{div } g)(v), \quad \text{for all } v \in \mathring{H}^1(\Omega),$$

where, since the distributional divergence of g is in $H^{-1}(\Omega)$, we have treated $f + \operatorname{div} g$ as a bounded linear functional on $\dot{H}^1(\Omega)$. By the inf-sup condition (40) and the Poincaré inequality, we have

$$\begin{aligned} \|u\|_{H^1(\Omega)} &\lesssim \sup_{v \in H^1(\Omega)} \frac{b_z(u, v)}{\|v\|_{H^1(\Omega)}} = \sup_{v \in H^1(\Omega)} \frac{(f + \operatorname{div} g)(v)}{\|v\|_{H^1(\Omega)}} \\ &\leq \|f\|_{H^{-1}(\Omega)} + \|\operatorname{div} g\|_{H^{-1}(\Omega)} \lesssim \|f\|_{L_2} + \|g\|_{L_2} \\ &\lesssim \|A_z(q, u)\|_{L_2}. \end{aligned}$$

Since $\mathcal{A}(q, u) = (g, f)$ also implies that $q + \nabla u = g$, the above inequality also implies

$$\begin{aligned} \|q\|_{L_2} &\leq \|g\|_{L_2} + \|\nabla u\|_{L_2} \lesssim \|f\|_{L_2} + \|g\|_{L_2} \\ &\lesssim \|A_z(q, u)\|_{L_2}^2. \end{aligned}$$

This proves (45). In particular, it shows that the operator A_z is continuous and injective. The equivalence of the weak formulation (38) and the boundary value problem (37) implies that A_z is also surjective. \square

Proposition 4.2. *The FOSLS resolvent approximation $R_h(z)$ converges in operator norm on V , i.e., Assumption 3.7 holds.*

Proof. Let $f \in V$, $u = R(z)f$, and $u_h = R_h(z)f$. Since $V_h \subset V$, by Galerkin orthogonality

$$\begin{aligned} \|A_z(q - q_h, u - u_h)\|_{L_2}^2 &= (A_z(q - q_h, u - u_h), A_z(q - r_h, u - w_h))_{L_2} \\ &\lesssim \|A_z(q - q_h, u - u_h)\|_{L_2} \left(\|q - r_h\|_{H(\operatorname{div})} + \|u - w_h\|_{H^1(\Omega)} \right). \end{aligned}$$

By standard finite element best approximation estimates for the Lagrange and Raviart-Thomas spaces, this leads to

$$\|A_z(q - q_h, u - u_h)\|_{L_2} \lesssim h^r |u|_{H^{r+1}(\Omega)} + h^r |q|_{H^r(\Omega)} + h^r |\operatorname{div} q|_{H^r(\Omega)} \quad (46)$$

for some $0 < r \leq 1$. Choosing $r \leq s$, where s is as in (41), the seminorms on the right hand side above can be bounded as follows:

$$\begin{aligned} |u|_{H^{r+1}(\Omega)} + |q|_{H^r(\Omega)} &\lesssim \|u\|_{H^{s+1}(\Omega)} \lesssim \|f\|_{\mathcal{H}} \lesssim \|f\|_V, \\ |\operatorname{div} q|_{H^r(\Omega)} &= |zu - f|_{H^r(\Omega)} \lesssim \|f\|_{H^r(\Omega)} \lesssim \|f\|_V, \end{aligned}$$

where in the last step we have used that $r \leq 1$ as well as the first bound for u . Using these estimates in (46),

$$\|A_z(q - q_h, u - u_h)\|_{L_2} \lesssim h^r \|f\|_V.$$

By Lemma 4.1, $\|u - u_h\|_{H^1(\Omega)}^2 + \|q - q_h\|_{L_2}^2 \leq \gamma_z \|A_z(q - q_h, u - u_h)\|_{L_2}^2$, so we conclude that for any $f \in V$,

$$\|R(z)f - R_h(z)f\|_V = \|u - u_h\|_{H^1(\Omega)} \leq \gamma_z^{1/2} \|A_z(q - q_h, u - u_h)\|_{L_2} \lesssim h^r \|f\|_V, \quad (47)$$

thus verifying Assumption 3.7 as $h \rightarrow 0$. \square

Proposition 4.3. *The FOSLS error estimator \mathcal{E} in (44) satisfies Assumption 3.9.*

Proof. Let $v_h \in V_h$ and $z \in \rho(\mathcal{A})$. Then $(q, u) = (R^q(z)v_h, R(z)v_h) \in X$ satisfies

$$A_z(q, u) = (0, v_h). \quad (48)$$

Let $(q_h, u_h) = (R_h^q(z)v_h, R_h(z)v_h) \in X_h$. By Lemma 4.1, as in (47),

$$\begin{aligned} \|R(z)f - R_h(z)f\|_V^2 &= \|u - u_h\|_{H^1}^2 \\ &\leq \gamma_z \|A_z(q - q_h, u - u_h)\|_{L_2}^2 && \text{by Lemma 4.1} \\ &= \gamma_z \|(0, v_h) - A_z(q_h, u_h)\|_{L_2}^2 && \text{by (48)} \\ &= \gamma_z \|(0, v_h) - A_z(R_h^q(z)v_h, R_h(z)v_h)\|_{L_2}^2. \end{aligned}$$

When this estimate is applied with $z = z_k$, the last term equals $\|\mathcal{E}_k v_h\|_{L_2}^2$. Hence collecting the estimates for all the poles z_k , by triangle inequality, we obtain $\|S_r v_h - S_{r,h} v_h\|_V \lesssim \|\mathcal{E} v_h\|_Y$, which verifies Assumption 3.9. \square

4.2. Eigenspace error estimation using DPG estimators. To define the DPG discretization of the resolvent applied to an $f \in \mathcal{H}$, reconsider the form $b_z(u, v)$ in (39) but now computing derivatives of v element-by-element and thereby extending it to v in the space of piecewise polynomials of degree $k + 3$ (without any interelement continuity), namely for v in

$$Y_h = \{v \in L_2(\Omega) : v|_K \in P^{k+3}(K) \text{ for all } K \in \Omega_h\}.$$

This is a subspace of the “broken” H^1 space $H^1(\Omega_h) := \prod_{K \in \Omega_h} H^1(K)$ where the inner product is

$$(v, y)_{H^1(\Omega_h)} = \sum_{K \in \Omega_h} \int_K v \bar{y} \, dx + \int_K \nabla v \cdot \nabla \bar{y} \, dx,$$

for any $v, y \in Y_h$, where again, the derivatives are computed element by element. Let n denote the unit outward normal vector on element boundaries and let $\widehat{X}_h = \{\widehat{r}_n : \text{on the boundary of every } K \in \Omega_h, \widehat{r}_n|_{\partial K} = (r \cdot n)|_{\partial K} \text{ for some } r \in RT_h\}$. Using the prior form $b_z(\cdot, \cdot)$ from (38), but now extended to $V \times Y_h$ as mentioned above, we define

$$a_z((w, \widehat{r}_n), v) = b_z(w, v) + \langle \widehat{r}_n, v \rangle_h$$

where

$$\langle \widehat{r}_n, v \rangle_h = \sum_{K \in \Omega_h} \int_{\partial K} \widehat{r}_n \bar{v} \, ds.$$

Given any $f \in L_2(\Omega)$, the DPG discretization of the resolvent problem $(z - \mathcal{A})u = f$ finds a $u_h \in V_h$, $\widehat{q}_n \in \widehat{X}_h$, and $\varepsilon_h \in Y_h$ such that

$$(\varepsilon_h, \delta_h)_{H^1(\Omega_h)} + a_z((u_h, \widehat{q}_n), \delta_h) = (f, \delta_h)_{L_2}, \quad (49a)$$

$$\overline{a_z((w_h, \widehat{r}_n), \varepsilon_h)} = 0, \quad (49b)$$

for all $\delta_h \in Y_h$ and $(w_h, \widehat{r}_n) \in V_h \times \widehat{X}_h$. This system, known as the primal DPG method, is well known to be uniquely solvable. The mapping from f to the solution component in V_h defines the DPG resolvent approximation $R_h(z) : \mathcal{H} \rightarrow V_h$. In addition, we also need the map to the ε_h solution component, which we denote by $R_h^\varepsilon(z)f := \varepsilon_h$, i.e.,

$$f \xrightarrow{R_h(z)} u_h \text{ solving (49)}, \quad f \xrightarrow{R_h^\varepsilon(z)} \varepsilon_h \text{ solving (49)}.$$

Using the resolvent approximation at each z_k , we define the DPG error estimator by

$$\mathcal{E} v_h = (R_h^\varepsilon(z_1)v_h, \dots, R_h^\varepsilon(z_N)v_h). \quad (50)$$

With Y set to the N -fold Cartesian product $Y = Y_h^N$, normed by the product $H^1(\Omega_h)$ -norm defined by

$$\|(y_1, \dots, y_N)\|_Y^2 = \sum_{k=1}^N \|y_k\|_{H^1(\Omega_h)}^2 = \sum_{k=1}^N \sum_{K \in \Omega_h} \|y_k\|_{H^1(K)}^2, \quad (51)$$

equation (50) defines $\mathcal{E} : V_h \rightarrow Y$ and completes the description of all DPG ingredients needed to fit the prior framework.

Proposition 4.4. *The DPG resolvent approximation converges in operator norm on V and Assumption 3.7 holds. Furthermore, the DPG error estimator \mathcal{E} , set in (50), satisfies Assumption 3.9.*

Proof. The proof of the first statement is very similar to the proof of [39, Lemma 3.4] so we omit it. To prove the statement on \mathcal{E} , we appeal to [27, Theorem 6.4] (see also [16]), noting that all assumptions required for that result are also essentially verified there (see e.g., [27, Example 4.2]). Hence the conclusion of that theorem on reliability of DPG error estimators give

$$\|R(z)v_h - R_h(z)v_h\|_V \lesssim \|\Pi\| \|R_h^\varepsilon(z)v_h\|_{H^1(\Omega_h)} + \text{osc}(v_h) \quad (52)$$

for any $z \in \rho(\mathcal{A})$ and $v_h \in V_h$, where

$$\text{osc}(v_h) = \sup_{y \in H^1(\Omega_h)} \frac{(v_h, y - \Pi y)_{L_2}}{\|y\|_{H^1(\Omega_h)}}.$$

Here $\Pi : H^1(\Omega_h) \rightarrow Y_h$ is a Fortin operator satisfying $a_z((w_h, \hat{r}_n), y - \Pi y) = 0$ for all $y \in H^1(\Omega_h)$, $w_h \in V_h$ and $\hat{r}_n \in \hat{X}_h$, whose operator norm admits a meshsize-independent bound, i.e., $\|\Pi\| \lesssim 1$, and satisfies the moment condition

$$\int_K (\Pi y - y)q \, dx = 0, \quad \text{for all } q \in P^k(K), \quad (53)$$

on all elements $K \in \Omega_h$, as well as further moment conditions on mesh edges—see e.g., [27, Theorem 5.4] or [41] for further details. Observe that for any $v_h \in V_h$,

$$(v_h, y - \Pi y)_{L_2} = 0$$

due to (53). Hence $\text{osc}(v_h) = 0$ and (52) implies

$$\|R(z_k)v_h - R_h(z_k)v_h\|_V \lesssim \|R_h^\varepsilon(z_k)v_h\|_{H^1(\Omega_h)}.$$

Hence the definition of \mathcal{E} in (50) and triangle inequality completes the verification of Assumption 3.9. \square

5. NUMERICAL RESULTS

In this section, we briefly present two numerical examples. The first concerns a selfadjoint Laplace eigenproblem on a interesting domain and falls within what is covered by the theory in Section 4. Here we report results on how the adaptive algorithm applied to two distinct eigenvalue clusters with different regularity profiles captures distinct refinement patterns for each. The second is a computational study of the proposed eigenspace error estimation technique applied to a nonselfadjoint Helmholtz eigenproblem for leaky waveguide modes. Here, the adaptive algorithm finds an almost circularly symmetric refinement pattern even though none of the two eigenmodes found have circular symmetry, indicating again that refinement patterns target the cluster as a whole and not solely individual eigenfunctions.

In both examples, we consider a discretization using the DPG method described in Section 4.2. We use the element-by-element definition of previously described eigenspace error estimator to design an h -adaptive mesh refinement algorithm in a standard fashion based on the SOLVE→ESTIMATE→MARK→REFINE paradigm (see, e.g., [65]), described further below. For adaptive mesh refinement, finite element assembly, and visualization, we use the NGSolve finite element library [63] and its implementation of Lagrange finite elements of polynomial degree $k = 5$. For an eigensolver, we use a simple Python implementation of the FEAST algorithm (available in [36]), which generates a sequence of eigenspace iterates that converge to the eigenspace approximation E_h , represented computationally by a set of basis vectors returned upon meeting a stopping criterion.

For the marking step in adaptivity, we employ a greedy strategy, based on the error estimator defined in Section 3. It is necessary to “localize” the error estimator $\mathcal{E} : V_h \rightarrow Y$ to each element K for this purpose. In all our examples, there is a natural space $Y(K)$ on each K such that

$$Y = \prod_{K \in \Omega_h} Y(K),$$

allowing \mathcal{E} to be split into local contributions. For instance, (51) in the DPG case shows that the norm of any $y = (y_1, \dots, y_N) \in Y$ with $y_k \in H^1(\Omega_h)$ can be written using

$$\|y\|_{Y(K)}^2 := \sum_{k=1}^N \|y_k\|_{H^1(K)}^2$$

as $\|y\|_Y^2 = \sum_{K \in \Omega_h} \|y\|_{Y(K)}^2$. Similarly, in the FOSLS case of (44), $y = \mathcal{E}v_h$ has N components $y_k = \mathcal{E}_k v_h$, $k = 1, \dots, N$, and we set $Y(K) = L_2(K)^N$ normed by

$$\|y\|_{Y(K)}^2 := \sum_{k=1}^N \|y_k\|_{L_2(K)}^2.$$

Using the local $Y(K)$ in each case, we define element-by-element error indicators η_K and accompanying quantities, namely let

$$\eta_K = \|\mathcal{E}v_h\|_{Y(K)}, \quad \eta_{\max} = \max_{K \in \Omega_h} \eta_K, \quad \text{and } \eta_{\ell^2} = \left(\sum_{K \in \Omega_h} \eta_K^2 \right)^{1/2},$$

be the local error indicator, the maximum error indicator, and the ℓ^2 -norm of the error indicators, respectively. Next, we say K is marked for refinement if, given a fixed ratio parameter $0 < \theta < 1$, $\eta_K \geq \theta \eta_{\max}$. Finally, we refine all marked elements using a standard conforming long-edge bisection algorithm. We set $\theta = 0.9$. Various other marking strategies can be employed, such as the Dörfler marking strategy [30]. However, we note that the greedy strategy is simple to implement and performs well in practice.

5.1. Laplace eigenproblem on a Gordon-Webb-Wolpert drum. Our first numerical example is the aforementioned Laplace eigenproblem on one of the Gordon-Webb-Wolpert (GWW) isospectral drums [42, 31]. This domain is one of two non-congruent planar domains that share the same Dirichlet Laplace spectrum (providing a negative answer to the famous question “Can one hear the shape of a drum?” posed by Kac [50]). We begin by computing a cluster of eigenvalues surrounding the ninth eigenvalue. We define a circular contour Γ_{cl} of center $c_{\text{cl}} = 12.33$ and radius $r_{\text{cl}} = 1.00$ which contains the eighth, ninth and tenth

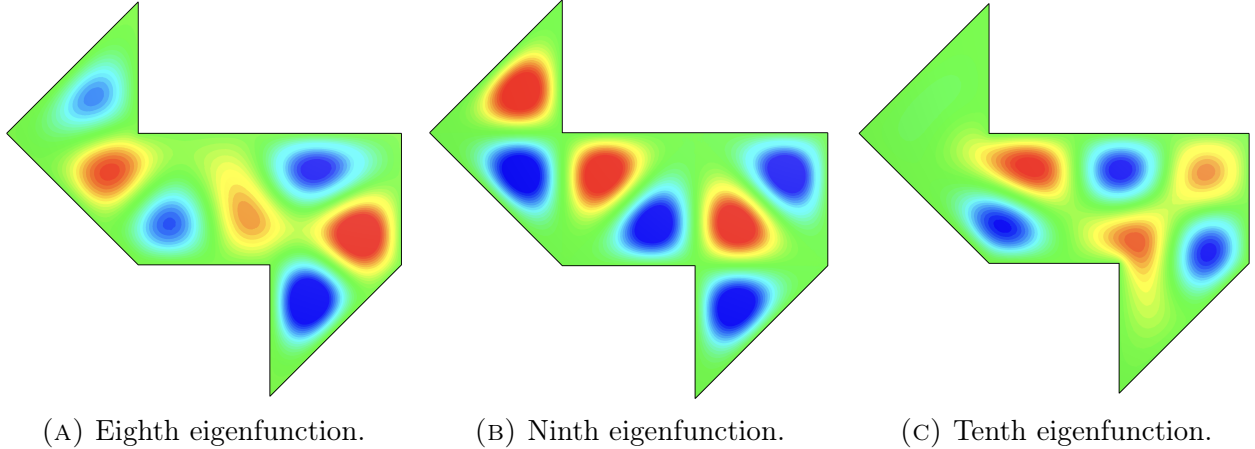


FIGURE 1. Eigenfunctions corresponding to the eighth, ninth and tenth eigenvalues (λ_8 , λ_9 and λ_{10}) of the Laplace operator a GWW isospectral drum. Scale varies between figures.

eigenvalues of the Laplace operator associated with both GWW domains. As reported in [31], the eighth, ninth and tenth eigenvalues of the Laplace operator on both GWW domains are approximately given by

$$\lambda_8 \approx 11.5413953956, \quad \lambda_9 \approx 12.3370055014, \quad \text{and} \quad \lambda_{10} \approx 13.0536540557.$$

We denote the cluster of eigenvalues contained in Γ_{cl} by $\Lambda_{\text{cl}} = \{\lambda_8, \lambda_9, \lambda_{10}\}$. Similarly, we define a circular contour Γ_{sg} of center $c_{\text{sg}} = 12.33$ and radius $r_{\text{sg}} = 0.4$ which contains only the ninth eigenvalue, and denote the corresponding cluster by $\Lambda_{\text{sg}} = \{\lambda_9\}$. Then we use the FEAST method that discretizes the contour integral by a four-point trapezoidal quadrature rule producing a rational function as in Example 3.6 with $N = 4$ (including the shift ϕ mentioned there to avoid poles on the real axis). Using the corresponding DPG error estimator \mathcal{E} , we run the adaptive algorithm. For the purpose of benchmarking, we also ran the adaptive algorithm using an explicit residual error estimator [55, Section 3.2] and a DWR error estimator [48, Equation (85)] (with a first-order weight given by the gradient of the computed eigenfunction). Note that these estimators were not designed for a cluster of eigenvalues, but we have adapted them to this setting by considering the element-wise sum of the error indicators for each eigenpair in the cluster.

The result, displayed in Figure 2, shows that the method is capable of automatically finding the right locations needing refinement. The initial mesh in Figure 2a is a quasi-uniform mesh with approximate mesh size $h = 0.3$. The final mesh in Figure 2c shows strong refinement near the re-entrant corners of the domain, where the eigenfunctions are known to be singular or to have larger gradients (see Figure 1). In contrast, the final mesh in Figure 2b shows uniform refinement in the whole domain, due to the regularity of the ninth eigenfunction (see Figure 1b).

In Figure 5, we show the convergence of the Hausdorff distance between the (approximated) cluster of known eigenvalues $\Lambda_{\text{cl}} = \{\lambda_8, \lambda_9, \lambda_{10}\}$ and their computed approximations $\Lambda_{h,\text{cl}}$. Similarly, in Figure 3, we show the convergence of the Hausdorff distance between the (approximated) known eigenvalue $\Lambda_{\text{sg}} = \{\lambda_9\}$ and its computed approximation $\Lambda_{h,\text{sg}}$. Recall that the Hausdorff distance between two sets $\Upsilon_1, \Upsilon_2 \subset \mathbb{C}$ is defined by $d(\Upsilon_1, \Upsilon_2) = \max\{\sup_{\mu_1 \in \Upsilon_1} \inf_{\mu_2 \in \Upsilon_2} |\mu_1 - \mu_2|, \sup_{\mu_2 \in \Upsilon_2} \inf_{\mu_1 \in \Upsilon_1} |\mu_1 - \mu_2|\}$. This distance is

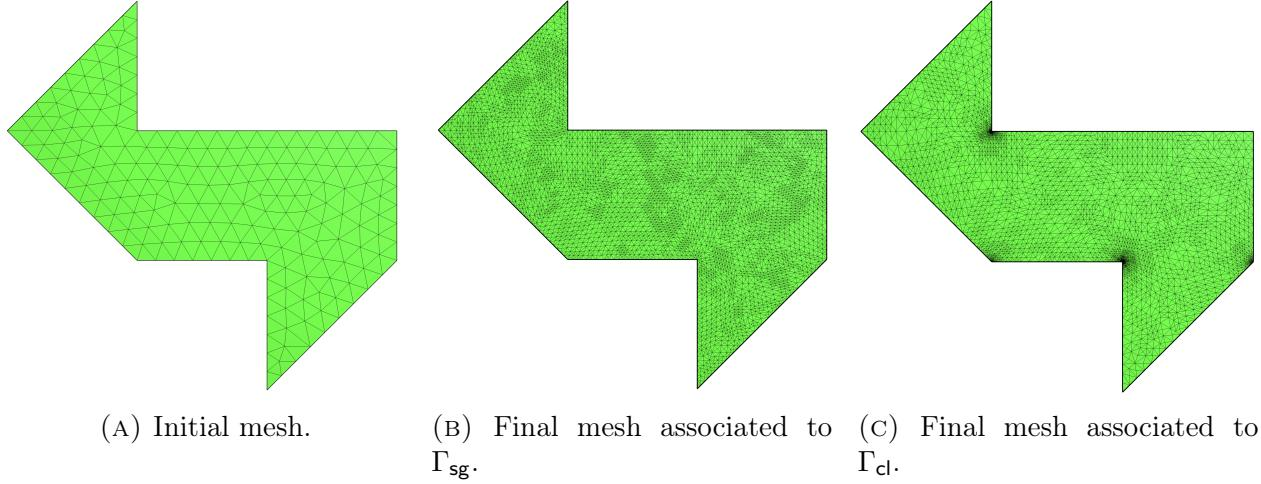


FIGURE 2. On the left, initial mesh on a GWW isospectral drum. On the center and right, final meshes after the adaptive algorithm, using the DPG error estimator for computing the single eigenvalue λ_9 (center) and the cluster Λ_{cl} (right).

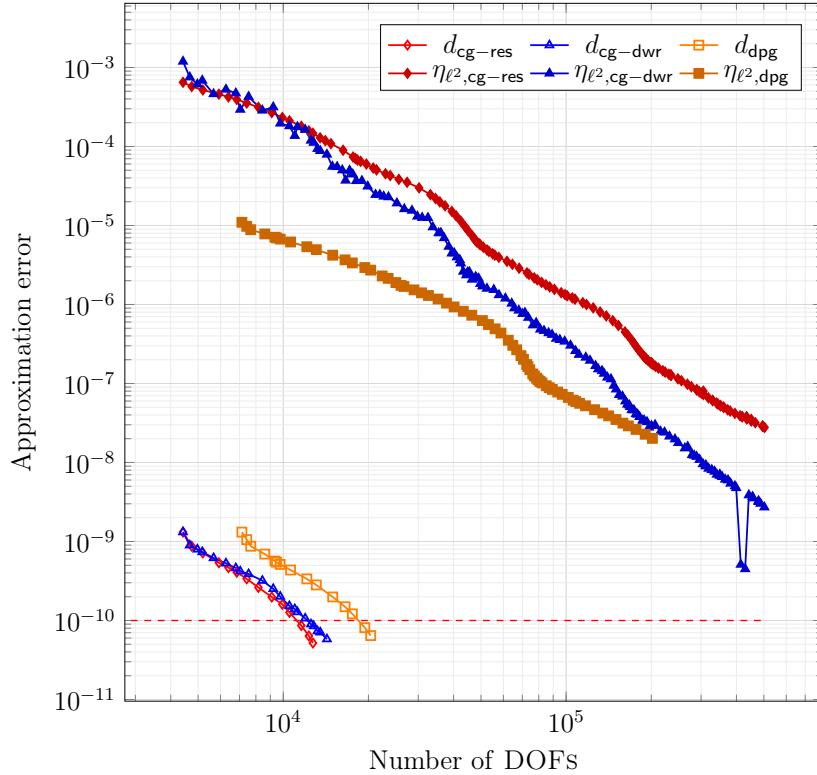


FIGURE 3. Hausdorff distance between the (approximated) ninth eigenvalue $\Lambda_{\text{sg}} = \{\lambda_9\}$ and its computed approximation, d_{\bullet} , and ℓ^2 -norm of the error estimator $\eta_{\ell^2,\bullet}$, for the different discretizations and error estimators ($\bullet \in \{\text{cg-res}, \text{cg-dwr}, \text{dpg}\}$), against the number of DOFs. The dashed red line indicates the level of accuracy of the reference eigenvalues.

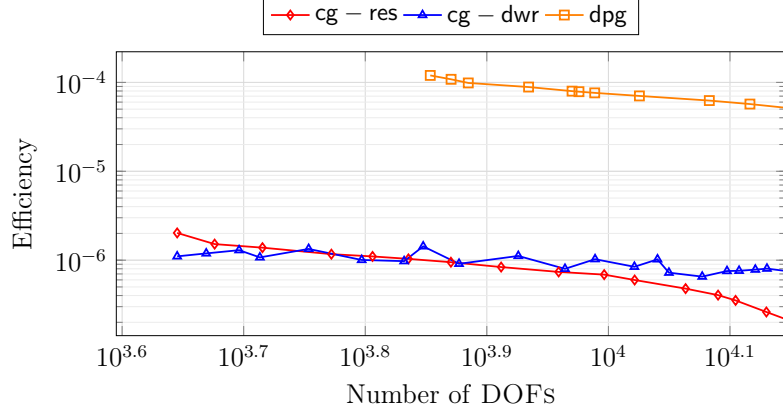


FIGURE 4. Efficiency ratio for the single eigenvalue approximation $\Lambda_{\text{sg}} = \{\lambda_9\}$, with different discretizations and error estimators ($\bullet \in \{\text{cg - res, cg - dwr, dpg}\}$), against the number of DOFs. (DOFs beyond 12,000 have been omitted for clarity.)

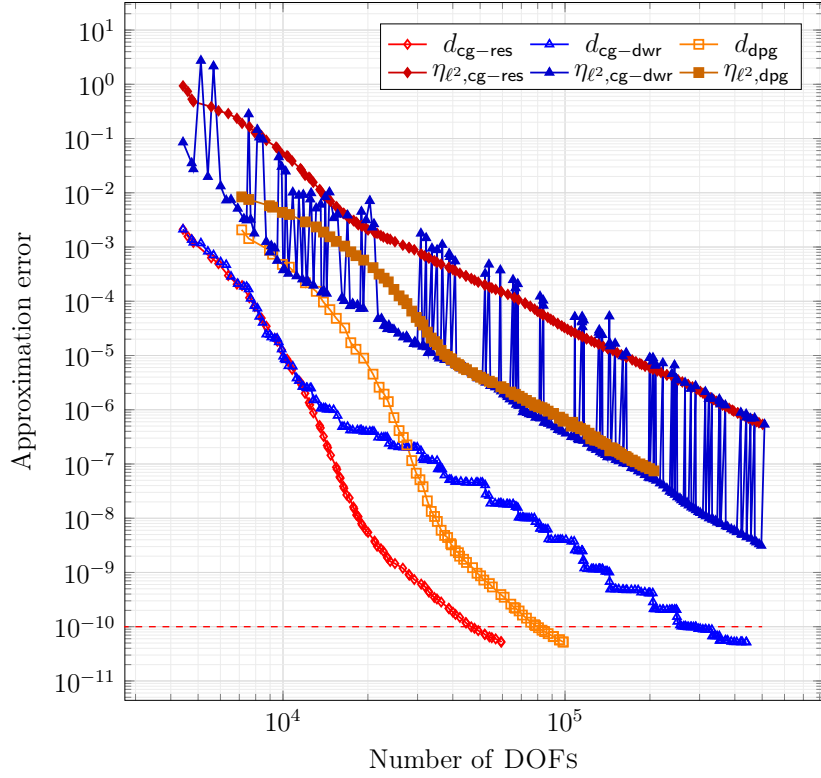


FIGURE 5. Hausdorff distance between the (approximated) cluster of known eigenvalues $\Lambda_{\text{cl}} = \{\lambda_8, \lambda_9, \lambda_{10}\}$ and the computed eigenvalues, d_{\bullet} , and ℓ^2 -norm of the error estimator $\eta_{\ell^2, \bullet}$, for the different discretizations and error estimators ($\bullet \in \{\text{cg - res, cg - dwr, dpg}\}$), against the number of DOFs. The dashed red line indicates the level of accuracy of the reference eigenvalues.

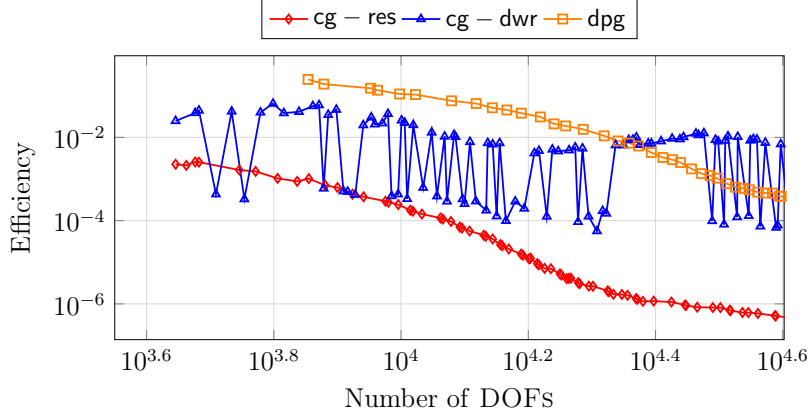


FIGURE 6. Efficiency ratio for the cluster eigenvalue approximation $\Lambda_{\text{cl}} = \{\lambda_8, \lambda_9, \lambda_{10}\}$, with different discretizations and error estimators ($\bullet \in \{\text{cg - res, cg - dwr, dpg}\}$), against the number of DOFs. (DOFs beyond 40,000 have been omitted for clarity.)

indicated by d in Figures 3, and 5 where the legends are subscripted by the discretization method, e.g., “ d_{dpg} ” denotes the method of Subsection 4.2, “ $d_{\text{cg-dwr}}$ ” denotes the above-mentioned DWR method with the standard Lagrange space discretization, and “ $d_{\text{cg-res}}$ ” denotes the Laplacian-specific explicit residual defined by Larson in [55]. The plots in the figure show how the error in eigenvalue cluster approximation and the ℓ^2 -norm of the error estimator decays as a function of the number of degrees of freedom (DOFs) as the mesh gets adaptively refined. The eigenvalue cluster error is measured by the Hausdorff distance between the set of approximate eigenvalues and the previously mentioned reference eigenvalues from [31]. Since the reference values are expected to be accurate to ten digits after the decimal point, a level of accuracy indicated in the figures by a dashed red line, eigenvalue errors lying below this line are not shown.

The explicit residual error estimator from [55] requires less degrees of freedom due to the nature of the underlying conforming discretization, while the DPG method uses a larger number of degrees of freedom due to the mixed formulation employed in our simulations. This leads to error curves (in Figures 3 and 5) that appear shifted to the right for the DPG method. Nonetheless, the DPG error estimator is tighter than the explicit residual error estimator and the (first-order) DWR error estimator, for both the cluster and the single eigenvalue cases, as can be observed in Figures 4 and 6. There, we plot an easily computable analogue of efficiency (that uses the eigenvalue cluster errors, which are more easily computed than the gap between eigenspaces), denoted by $\eta_{\ell^2, \bullet}$, defined as the ratio between the Hausdorff distance d_{\bullet} and the ℓ^2 -norm of the error estimator $\eta_{\ell^2, \bullet}$, i.e.,

$$\text{Eff}_{\ell^2, \bullet} = \frac{d_{\bullet}}{\eta_{\ell^2, \bullet}},$$

for $\bullet \in \{\text{cg - res, cg - dwr, dpg}\}$. Since the estimators $\eta_{\ell^2, \bullet}$ track the eigenspace error, we have little reason to expect $\text{Eff}_{\ell^2, \bullet}$ to be close to the perfect value of one, yet it is interesting to see how its values from our experiments. Note from Figures 4 and 6 that the DPG efficiency tends to bound the remaining two efficiency curves from above, indicating a tighter estimator, in the case of the single eigenvalue (Figure 4). We have truncated the plot to a maximum

of 12,000 DOFs to avoid the region where the methods may achieve greater accuracy than the reference eigenvalue. In the case of the cluster, the DPG case initially provides a tighter estimator, but as the number of DOFs increases, the DWR estimator becomes slightly tighter (Figure 6), yet it oscillates more than the DPG estimator. This phenomenon has been observed in our previous work [37] for a similar (Maxwell) DWR estimator for a cluster of eigenvalues. Similar simulations for the Laplace eigenproblem on the GWW domain were performed considering the DWR error estimator with second-order derivative weights (not reported here), yielding efficiency curves with similar oscillatory behavior. A more cluster-robust DWR estimator might need to be developed to overcome this issue (instead of our simple generalization of singleton DWR estimator). In these plots, as in the single eigenvalue case, we have truncated the plot to a maximum of 40,000 DOFs to avoid the region where the methods may achieve greater accuracy than the reference eigenvalues.

5.2. Helmholtz eigenproblem on a Bragg fiber. For our second numerical example, we consider the Helmholtz eigenproblem for a leaky mode. Leaky modes are slightly lossy, yet are very important practically to guide light through modern microstructured fibers. (For some examples of such fibers, see [37].) These modes satisfy an outgoing boundary condition at infinity permitting the leakage of energy which makes the corresponding eigenproblem nonselfadjoint. Here we consider a simple model fiber, the Bragg fiber, which is often used to get intuition for more complex fibers. We handle the outgoing condition by inserting a perfectly matched layer (PML) [5, 22, 10] which modifies the solution within that layer to a decaying one (while leaving the solution unchanged in the remainder) allowing us to truncate the infinite-domain problem to a bounded computational domain Ω . The purpose of this subsection is to present a computational study of the performance of the proposed DPG error estimator for this nonselfadjoint eigenproblem. (A full verification of Assumption 3.7 for this case requires further advances in DPG theory which will take us too far away from the present focus.)

The equation for the Helmholtz eigenproblem on the transverse fiber cross section, after subtracting off the homogenous refractive index n_0 of the infinite air surround, and after a nondimensionalization by a characteristic length scale L , becomes (see e.g., [40, Eq. (21a–b)])

$$\begin{aligned} -\Delta u + Vu = Z^2 u, \quad & \text{in } \mathbb{R}^2, \\ u \text{ is outgoing as } r = \sqrt{x_0^2 + x_1^2} \rightarrow \infty, \end{aligned} \tag{54}$$

where V is the *index well* defined by $V(x) = L^2 k^2 (n_0^2 - n^2(x))$, $k \in \mathbb{R}$ is the operational wavenumber, $n = n(x)$ is the refractive index profile of the fiber, and Z^2 is the nondimensionalized eigenvalue to be found. In terms of the physical “propagation constant” β , the original Helmholtz eigenvalue is β^2 , and the nondimensional eigenvalue is $Z^2 = L^2 (k^2 n_0^2 - \beta^2)$.

To truncate the domain using a PML, we perform a complex change of variables $\tilde{x} = \Phi(x)$ where $\Phi(x) := \frac{\eta(r)}{r} x$ with complex-valued function $\eta : \mathbb{R}_{\geq 0} \rightarrow \mathbb{C}$, defined shortly, of the radial coordinate r . The map Φ is the identity on the disk $r < r_0$, while for $r > r_0$ it is designed to transform the solution to an exponentially decaying function of r . It is standard (see e.g., [22]) to transform the problem (54) to $\mathcal{A}u = Z^2 u$, where the operator \mathcal{A} now depends on Φ , and then truncate the domain to a finite domain Ω of some radius sufficiently greater than r_0 where the transformed mode u has decayed enough to be indistinguishable from zero. Using this \mathcal{A} , the following modified DPG discretization of the resolvent problem $(Z^2 - \mathcal{A})u = f$

on Ω is obtained: find $u_h \in V_h$, $\hat{q}_n \in \hat{X}_h$ such that

$$(\varepsilon_h, \delta_h)_{H^1(\Omega_h)} + a_{Z^2, \text{PML}}((u_h, \hat{q}_n), \delta_h) = (\det(J)f, \delta_h)_{L_2(\Omega)}, \quad (55)$$

$$\overline{a_{Z^2, \text{PML}}((w_h, \hat{r}_n), u_h)} = 0, \quad (56)$$

for all $\delta_h \in Y_h$ and $(w_h, \hat{r}_n) \in V_h \times \hat{X}_h$, where

$$\begin{aligned} a_{Z^2, \text{PML}}((u, \hat{q}_n), v) = & Z^2(\det(J)u, v)_{L_2} - (\gamma \nabla u, \nabla v)_{L_2} \\ & - (\det(J)Vu, v)_{L_2} + \langle \det(J)J^{-\top} \hat{q}_n, v \rangle_h \end{aligned} \quad (57)$$

for all $v \in Y_h$, where J denotes the Jacobian matrix of the transformation Φ , and $\gamma = J^{-1}J^{-\top} \det(J)$.

There are multiple ways to choose the mapped radius $\eta(r)$, as previously observed in the literature [22, 40, 53, 59]. We use a two-dimensional analogue of an expression in [53] (see also [37]). For simplicity, fix Ω to be a disk of radius r_1 . Furthermore, assume that support of the index well V is contained in a disk of radius $r_0 < r_1$, and that a cylindrical PML is set in the annular region $r_0 < r < r_1$. Let $0 < \alpha$ be the PML strength parameter. We set

$$\eta(r) = r(1 + i\phi(r)), \quad (58a)$$

where

$$\phi(r) = \begin{cases} 0, & \text{if } r < r_0, \\ \alpha \frac{\int_{r_0}^r (s - r_0)^2(s - r_1)^2 ds}{\int_{r_0}^{r_1} (s - r_0)^2(s - r_1)^2 ds}, & \text{if } r_0 < r < r_1. \end{cases} \quad (58b)$$

This together with $\zeta(r) = \eta(r)/r$ defines all quantities required to compute the Jacobian J of the transformation Φ .

For the purpose of this example, we consider a simple Bragg fiber (see [37, Section 4], and references therein), with coefficients defined by Table 1. The geometry of the fiber is illustrated in Figure 7a. The initial mesh in Figure 7b is a quasi-uniform mesh with approximate element size $h \approx 1.0$ for the PML region, and $h \approx 0.1$ for the inner fiber region. We approximate an exact eigenvalue of multiplicity two, i.e., the exact cluster Λ is a singleton containing $Z^2 = 2.0302671 + i0.0024486$, a reference value obtained by semianalytical computations. (The corresponding two eigenfunctions have patterns similar to the standard two-leaved linearly polarized LP_{11} -like guided modes within the core, but they are leaky modes.) The associated discrete cluster Λ_h is computed using the FEAST method, with a circular contour Γ centered at the exact eigenvalue and radius $r_\Gamma = 0.1$, and usually has two elements, both close to the exact eigenvalue.

Figure 7c displays the final mesh after running the adaptive algorithm using the DPG error estimator for approximating the second fundamental eigenvalue cluster. Observe that the refinement is concentrated in the glass cladding of the fiber. This is in concordance with the oscillatory fine structures observed in [64], and depicted in Figures 8b and 8d, where the scalar components of the eigenmodes are rescaled to better visualize the behavior in the glass ring. Figures 8a and 8c display the same eigenmodes without rescaling, showing how the modes are mostly confined to the air core of the fiber. The performance of the DPG error estimator is illustrated in Figure 9, where we plot the convergence of the Hausdorff distance

Name	Symbol	Value
Nondimensionalization length scale	L	1.5×10^{-5} m
Operating wavenumber	k	$\frac{2\pi}{1.7} \times 10^6$ m ⁻¹
Refractive index in air regions	n_{air}	1.00027717
Refractive index in glass ring	n_{glass}	1.43881648
Air core radius	r_{core}	2.7183
Outer radius of glass ring	r_{outer}	3.385
Thickness of glass ring	t_{ring}	0.66666667
Outer radius of outer air region	r_0	4.385
Thickness of outer air region	t_{air}	1.0
Outer radius of PML	r_1	8.05166666
Thickness of PML	t_{PML}	3.66666667
PML strength	α	10.0

TABLE 1. Parameters defining the Bragg fiber used in the numerical experiments.

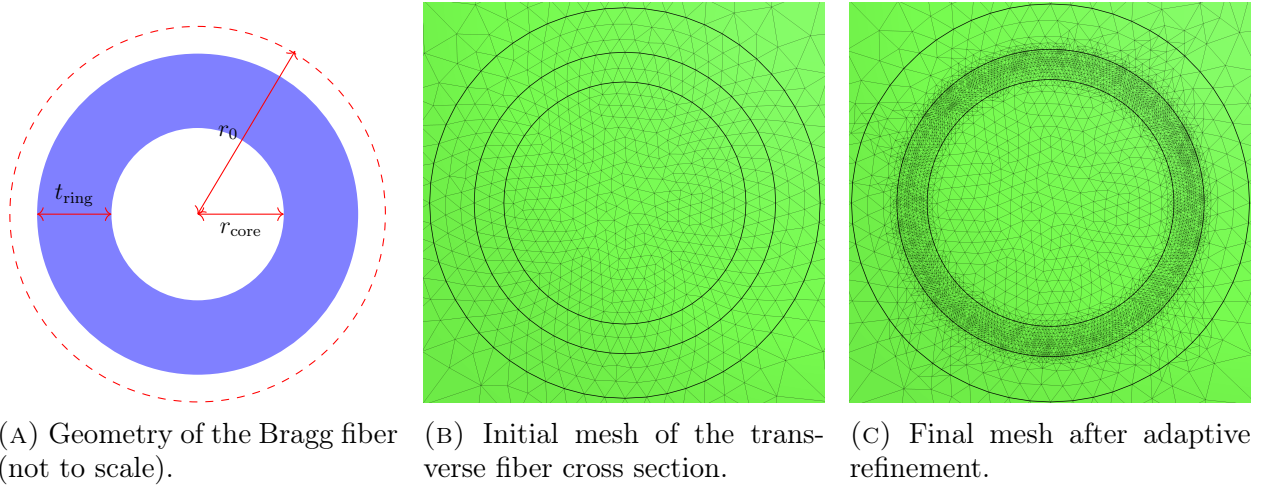


FIGURE 7. Geometry of the Bragg fiber (left), initial mesh (center), and final mesh after adaptive refinement (right) using the DPG error estimator for approximating the second fundamental eigenvalue cluster.

between the exact eigenvalue cluster Λ and its computed approximation Λ_h , as well as the ℓ^2 -norm of the DPG error estimator, against the number of degrees of freedom.

Acknowledgments. This work was supported in part by the NSF grant DMS-2245077. It also benefited from activities organized under the auspices of NSF RTG grant DMS-2136228.

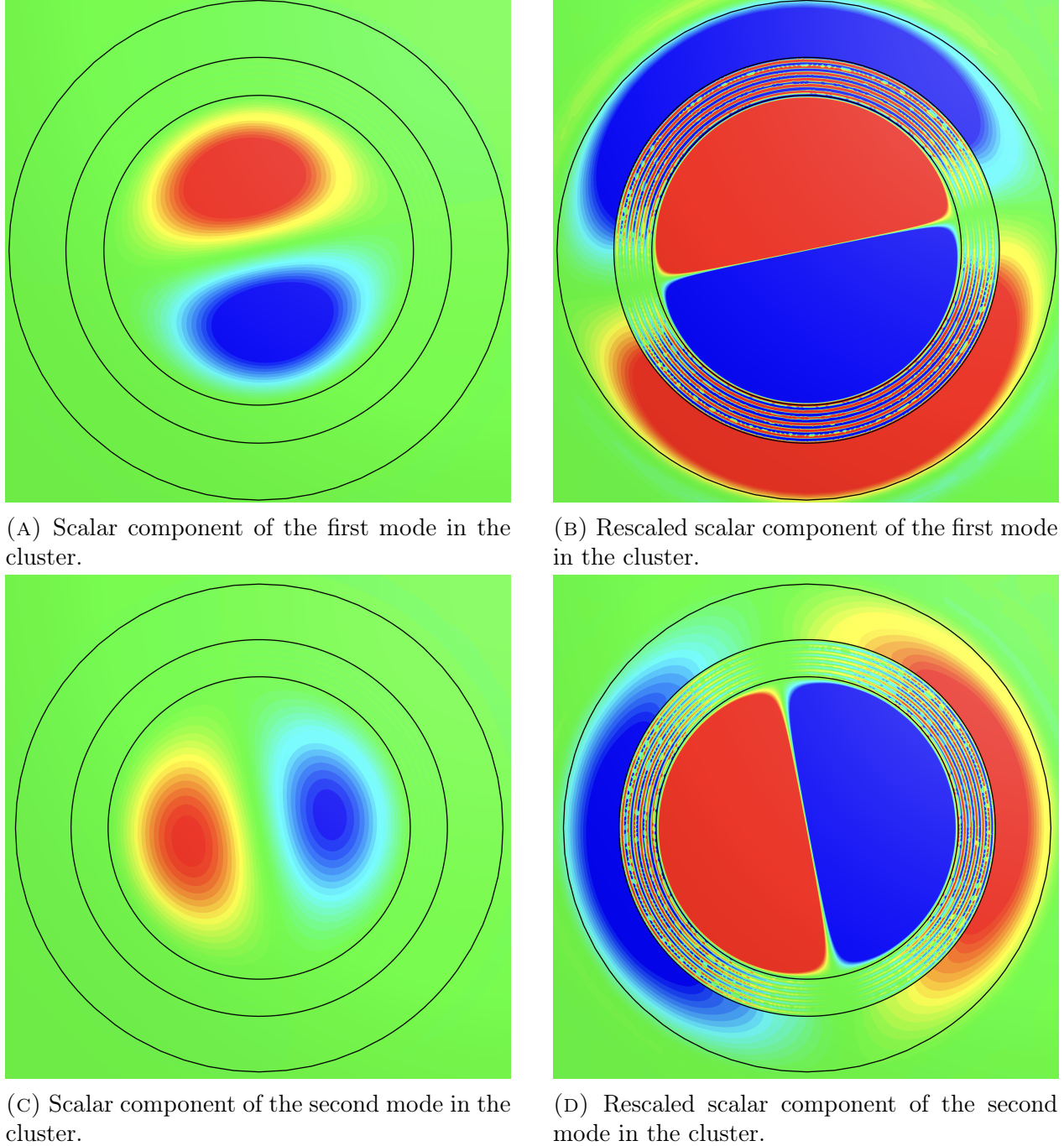


FIGURE 8. Two Bragg eigenmodes of the computed cluster are shown in different color scales in the left column and right column. The color scale of right column is selected for better visualization of the oscillatory features in the cladding region.

REFERENCES

[1] M. AINSWORTH AND J. T. ODEN, *A posteriori error estimation in finite element analysis*, Computer methods in applied mechanics and engineering, 142 (1997), pp. 1–88.

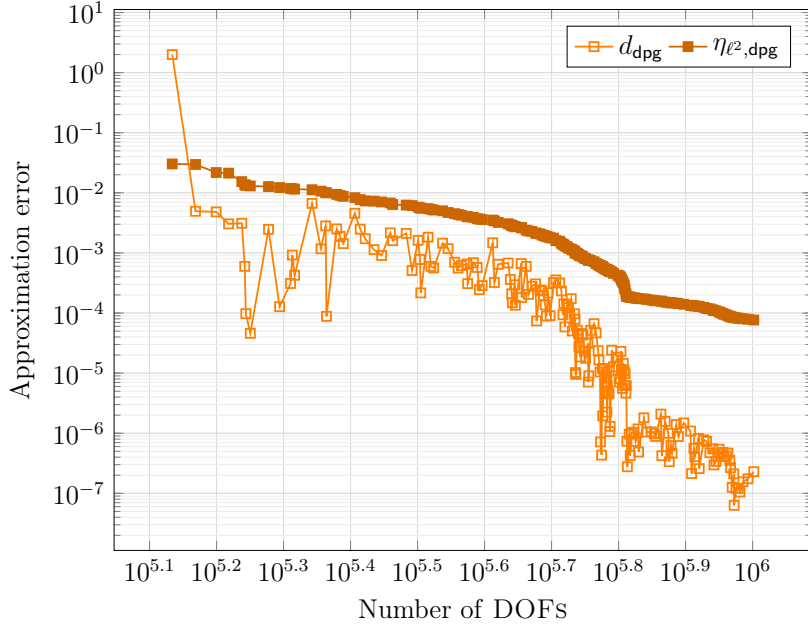


FIGURE 9. Hausdorff distance between the (approximated) eigenvalue cluster $\Lambda = \{Z^2\}$ and its computed approximation, d_{dpg} , and ℓ^2 -norm of the DPG error estimator $\eta_{\ell^2,\text{dpg}}$, against the number of DOFs.

- [2] I. BABUŠKA AND W. RHEINBOLDT, *Adaptive approaches and reliability estimations in finite element analysis*, Computer Methods in Applied Mechanics and Engineering, 17 (1979), pp. 519–540.
- [3] I. BABUŠKA AND W. C. RHEINBOLDT, *A-posteriori error estimates for the finite element method*, International journal for numerical methods in engineering, 12 (1978), pp. 1597–1615.
- [4] R. E. BANK, L. GRUBIŠIĆ, AND J. S. OVALL, *A framework for robust eigenvalue and eigenvector error estimation and Ritz value convergence enhancement*, Applied numerical mathematics, 66 (2013), pp. 1–29.
- [5] J.-P. BERENGER, *A perfectly matched layer for the absorption of electromagnetic waves*, Journal of computational physics, 114 (1994), pp. 185–200.
- [6] F. BERTRAND AND D. BOFFI, *Least-squares formulations for eigenvalue problems associated with linear elasticity*, Computers & Mathematics with Applications, 95 (2021), pp. 19–27.
- [7] F. BERTRAND AND D. BOFFI, *First order least-squares formulations for eigenvalue problems*, IMA Journal of Numerical Analysis, 42 (2022), pp. 1339–1363.
- [8] P. B. BOCHEV AND M. D. GUNZBURGER, *Least-squares finite element methods*, vol. 166 of Applied Mathematical Sciences, Springer, New York, 2009.
- [9] D. BOFFI, *Finite element approximation of eigenvalue problems*, Acta Numerica, 19 (2010), pp. 1–120.
- [10] J. BRAMBLE AND J. PASCIAK, *Analysis of a finite pml approximation for the three dimensional time-harmonic maxwell and acoustic scattering problems*, Mathematics of Computation, 76 (2007), pp. 597–614.
- [11] F. BREZZI AND M. FORTIN, *Mixed and hybrid finite element methods*, vol. 15, Springer Science & Business Media, 2012.
- [12] Z. CAI, R. LAZAROV, T. A. MANTEUFFEL, AND S. F. MCCORMICK, *First-order system least squares for second-order partial differential equations: Part I*, SIAM Journal on Numerical Analysis, 31 (1994), pp. 1785–1799.
- [13] Z. CAI, T. A. MANTEUFFEL, AND S. F. MCCORMICK, *First-order system least squares for second-order partial differential equations: Part II*, SIAM Journal on Numerical Analysis, 34 (1997), pp. 425–454.

- [14] E. CANCÈS, G. DUSSON, Y. MADAY, B. STAMM, AND M. VOHRALÍK, *Guaranteed and robust a posteriori bounds for laplace eigenvalues and eigenvectors: conforming approximations*, SIAM Journal on Numerical Analysis, 55 (2017), pp. 2228–2254.
- [15] ———, *Guaranteed a posteriori bounds for eigenvalues and eigenvectors: multiplicities and clusters*, Mathematics of Computation, 89 (2020), pp. 2563–2611.
- [16] C. CARSTENSEN, L. DEMKOWICZ, AND J. GOPALAKRISHNAN, *A posteriori error control for DPG methods*, SIAM Journal on Numerical Analysis, 52 (2014), pp. 1335–1353.
- [17] C. CARSTENSEN, D. GALLISTL, AND M. SCHEDENSACK, *Adaptive nonconforming Crouzeix-Raviart FEM for eigenvalue problems*, Mathematics of Computation, 84 (2015), pp. 1061–1087.
- [18] C. CARSTENSEN AND J. GEDICKE, *An oscillation-free adaptive FEM for symmetric eigenvalue problems*, Numerische Mathematik, 118 (2011), pp. 401–427.
- [19] ———, *Guaranteed lower bounds for eigenvalues*, Mathematics of Computation, 83 (2014), pp. 2605–2629.
- [20] C. CARSTENSEN, J. GEDICKE, V. MEHRMANN, AND A. MIEDLAR, *An adaptive homotopy approach for non-selfadjoint eigenvalue problems*, Numerische Mathematik, 119 (2011), pp. 557–583.
- [21] C. CARSTENSEN, Q. ZHAI, AND R. ZHANG, *A skeletal finite element method can compute lower eigenvalue bounds*, SIAM Journal on Numerical Analysis, 58 (2020), pp. 109–124.
- [22] F. COLLINO AND P. MONK, *The perfectly matched layer in curvilinear coordinates*, SIAM Journal on Scientific Computing, 19 (1998), pp. 2061–2090.
- [23] J. B. CONWAY, *Functions of one complex variable I*, vol. 11, Springer New York, NY, 2012.
- [24] L. DEMKOWICZ AND J. GOPALAKRISHNAN, *A class of discontinuous Petrov-Galerkin methods. Part II: Optimal test functions*, Numerical Methods for Partial Differential Equations, 27 (2011), pp. 70–105.
- [25] L. DEMKOWICZ AND J. GOPALAKRISHNAN, *A primal DPG method without a first-order reformulation*, Computers & Mathematics with Applications, 66 (2013), pp. 1058–1064.
- [26] L. DEMKOWICZ AND J. GOPALAKRISHNAN, *Discontinuous Petrov-Galerkin (DPG) method*, Encyclopedia of Computational Mechanics, 2 (2017), pp. 777–792.
- [27] ———, *The discontinuous Petrov-Galerkin method*, Acta Numerica, 34 (2025), pp. 293–384.
- [28] L. DEMKOWICZ, J. GOPALAKRISHNAN, AND A. NIEMI, *A class of discontinuous Petrov-Galerkin methods. Part III: Adaptivity*, Applied Numerical Mathematics, 62 (2012), pp. 396–427.
- [29] P. DÍEZ, J. J. EGOZCUE, AND A. HUERTA, *A posteriori error estimation for standard finite element analysis*, Computer Methods in Applied Mechanics and Engineering, 163 (1998), pp. 141–157.
- [30] W. DÖRFLER, *A robust adaptive strategy for the nonlinear Poisson equation*, Computing, 55 (1995), pp. 289–304.
- [31] T. A. DRISCOLL, *Eigenmodes of isospectral drums*, Siam Review, 39 (1997), pp. 1–17.
- [32] A. ERN, J.-L. GUERMOND, ET AL., *Finite elements II*, Springer, 2021.
- [33] S. GIANI, L. GRUBIŠIĆ, H. HAKULA, AND J. S. OVALL, *A posteriori error estimates for elliptic eigenvalue problems using auxiliary subspace techniques*, Journal of Scientific Computing, 88 (2021), pp. 1–25.
- [34] S. GIANI, L. GRUBIŠIĆ, A. MIEDLAR, AND J. S. OVALL, *Robust error estimates for approximations of non-self-adjoint eigenvalue problems*, Numerische Mathematik, 133 (2016), pp. 471–495.
- [35] S. GIANI, L. GRUBIŠIĆ, AND J. S. OVALL, *Benchmark results for testing adaptive finite element eigenvalue procedures part 2 (conforming eigenvector and eigenvalue estimates)*, Applied Numerical Mathematics, 102 (2016), pp. 1–16.
- [36] J. GOPALAKRISHNAN ET AL., *Pythonic FEAST*. <https://bitbucket.org/jayggg/pyeigfeast/>, 2025.
- [37] J. GOPALAKRISHNAN, J. GROSEK, G. PINOCHET-SOTO, AND P. VANDENBERGE, *Adaptive resolution of fine scales in modes of microstructured optical fibers*, SIAM Journal on Scientific Computing, 47 (2025), pp. B108–B130.
- [38] J. GOPALAKRISHNAN, L. GRUBIŠIĆ, AND J. OVALL, *Spectral discretization errors in filtered subspace iteration*, Mathematics of computation, 89 (2020), pp. 203–228.
- [39] J. GOPALAKRISHNAN, L. GRUBIŠIĆ, J. OVALL, AND B. PARKER, *Analysis of FEAST spectral approximations using the DPG discretization*, Computational methods in applied mathematics, 19 (2019), pp. 251–266.
- [40] J. GOPALAKRISHNAN, B. Q. PARKER, AND P. VANDENBERGE, *Computing leaky modes of optical fibers using a FEAST algorithm for polynomial eigenproblems*, Wave Motion, 108 (2022), p. 102826.

- [41] J. GOPALAKRISHNAN AND W. QIU, *An analysis of the practical DPG method*, Mathematics of Computation, 83 (2014), pp. 537–552.
- [42] C. GORDON, D. WEBB, AND S. WOLPERT, *Isospectral plane domains and surfaces via riemannian orbifolds*, Inventiones mathematicae, 110 (1992), pp. 1–22.
- [43] R. E. GREENE AND S. G. KRANTZ, *Function theory of one complex variable*, American Mathematical Soc., 2006.
- [44] P. GRISVARD, *Elliptic Problems in Nonsmooth Domains*, no. 24 in Monographs and Studies in Mathematics, Pitman Advanced Publishing Program, Marshfield, Massachusetts, 1985.
- [45] L. GRUBIŠIĆ AND J. OVALL, *On estimators for eigenvalue/eigenvector approximations*, Mathematics of computation, 78 (2009), pp. 739–770.
- [46] H. HAKULA, M. NEILAN, AND J. S. OVALL, *A posteriori estimates using auxiliary subspace techniques*, Journal of Scientific Computing, 72 (2017), pp. 97–127.
- [47] R. W. HAMMING, *Digital filters*, Courier Corporation, 1998.
- [48] V. HEUVELINE AND R. RANNACHER, *A posteriori error control for finite element approximations of elliptic eigenvalue problems*, Advances in Computational Mathematics, 15 (2001), pp. 107–138.
- [49] E. HILLE AND R. S. PHILLIPS, *Functional analysis and semi-groups*, vol. 31, American Mathematical Soc., 1996.
- [50] M. KAC, *Can one hear the shape of a drum?*, The American Mathematical Monthly, 73 (1966), pp. 1–23.
- [51] T. KATO, *Perturbation theory for linear operators*, vol. 132, Springer Science & Business Media, 2013.
- [52] J. KESTYN, E. POLIZZI, AND P. T. PETER TANG, *FEAST eigensolver for non-Hermitian problems*, SIAM Journal on Scientific Computing, 38 (2016), pp. S772–S799.
- [53] S. KIM AND J. PASCIAK, *The computation of resonances in open systems using a perfectly matched layer*, Mathematics of Computation, 78 (2009), pp. 1375–1398.
- [54] S. LANG, *Algebra*, vol. 211, Springer Science & Business Media, 2012.
- [55] M. G. LARSON, *A posteriori and a priori error analysis for finite element approximations of self-adjoint elliptic eigenvalue problems*, SIAM journal on numerical analysis, 38 (2000), pp. 608–625.
- [56] X. LIU AND T. VEJCHODSKÝ, *Fully computable a posteriori error bounds for eigenfunctions*, Numerische Mathematik, 152 (2022), pp. 183–221.
- [57] MANUEL GONZALEZ AND VICTOR M. ONIEVA, *On the meromorphic and Schechter-Shapiro operational calculi*, Journal of Mathematical Analysis and Applications, 116 (1986), pp. 363–377.
- [58] A. NAGA, Z. ZHANG, AND A. ZHOU, *Enhancing eigenvalue approximation by gradient recovery*, SIAM Journal on Scientific Computing, 28 (2006), pp. 1289–1300.
- [59] L. NANNEN AND M. WEISS, *Computing scattering resonances using perfectly matched layers with frequency dependent scaling functions*, BIT Numerical Mathematics, 58 (2018), pp. 373–395.
- [60] P. T. PETER TANG AND E. POLIZZI, *FEAST as a subspace iteration eigensolver accelerated by approximate spectral projection*, SIAM Journal on Matrix Analysis and Applications, 35 (2014), pp. 354–390.
- [61] E. POLIZZI, *Density-matrix-based algorithm for solving eigenvalue problems*, Physical Review B—Condensed Matter and Materials Physics, 79 (2009), p. 115112.
- [62] R. RANNACHER, A. WESTENBERGER, AND W. WOLLNER, *Adaptive finite element solution of eigenvalue problems: balancing of discretization and iteration error*, (2010).
- [63] J. SCHÖBERL ET AL., *Netgen/NGSolve*. <https://ngsolve.org>, 2025.
- [64] P. VANDENBERGE, J. GOPALAKRISHNAN, AND J. GROSEK, *Sensitivity of confinement losses in optical fibers to modeling approach*, Optics Express, 31 (2023), pp. 26735–26756.
- [65] VERFÜRTH, RÜDIGER, *A posteriori error estimation and adaptive mesh-refinement techniques*, Journal of Computational and Applied Mathematics, 50 (1994), pp. 67–83.
- [66] T. YAMAMOTO, *A note on the spectral mapping theorem*, SIAM Journal on Mathematical Analysis, 2 (1971), pp. 49–51.
- [67] O. C. ZIENKIEWICZ AND J. Z. ZHU, *The superconvergent patch recovery and a posteriori error estimates. Part 1: The recovery technique*, International Journal for Numerical Methods in Engineering, 33 (1992), pp. 1331–1364.
- [68] ———, *The superconvergent patch recovery and a posteriori error estimates. Part 2: Error estimates and adaptivity*, International Journal for Numerical Methods in Engineering, 33 (1992), pp. 1365–1382.